

FedDifRC: Unlocking the Potential of Text-to-Image Diffusion Models in Heterogeneous Federated Learning

Huan Wang^{1,*}, Haoran Li^{1,3,*}, Huaming Chen², Jun Yan¹, Jiahua Shi³, Jun Shen^{1,†}

¹School of Computing and Information Technology, University of Wollongong, Wollongong, Australia

²School of Electrical and Computer Engineering, The University of Sydney, Sydney, Australia

³QLD Alliance for Agriculture and Food Innovation, The University of Queensland, Brisbane, Australia

hw226@uowmail.edu.au

*Equal Contribution

†Corresponding Author

Abstract

Federated learning aims at training models collaboratively across participants while protecting privacy. However, one major challenge for this paradigm is the data heterogeneity issue, where biased data preferences across multiple clients, harming the model’s convergence and performance. In this paper, we first introduce powerful diffusion models into the federated learning paradigm and show that diffusion representations are effective steers during federated training. To explore the possibility of using diffusion representations in handling data heterogeneity, we propose a novel diffusion-inspired **Federated** paradigm with **Diffusion Representation Collaboration**, termed **FedDifRC**, leveraging meaningful guidance of diffusion models to mitigate data heterogeneity. The key idea is to construct text-driven diffusion contrasting and noise-driven diffusion regularization, aiming to provide abundant class-related semantic information and consistent convergence signals. On the one hand, we exploit the conditional feedback from the diffusion model for different text prompts to build a text-driven contrastive learning strategy. On the other hand, we introduce a noise-driven consistency regularization to align local instances with diffusion denoising representations, constraining the optimization region in the feature space. In addition, **FedDifRC** can be extended to a self-supervised scheme without relying on any labeled data. We also provide a theoretical analysis for **FedDifRC** to ensure convergence under non-convex objectives. The experiments on different scenarios validate the effectiveness of **FedDifRC** and the efficiency of crucial components. Code is available at <https://github.com/hwang52/FedDifRC>.

1. Introduction

Federated Learning (FL) [35] has become increasingly popular as a decentralized training paradigm, with multiple distributed clients train their local models without sharing their

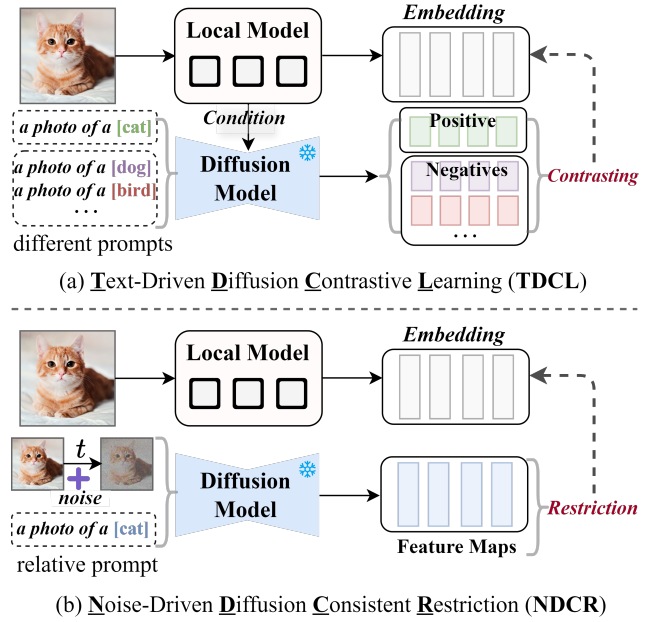


Figure 1. The main idea of **FedDifRC** with two key modules **TDCL** and **NDCR**. (a) We leverage conditional generative feedback of the pre-trained diffusion model on various text prompts to devise a *text-driven contrastive learning* strategy, where the input embedding is injected as a condition. (b) We extract the diffusion denoising feature maps of intermediate layers from the pre-trained diffusion model at a specific time step t during the diffusion backward process to construct a *noise-driven regularization*.

private dataset [17, 29] (i.e., training client models locally and aggregating them globally [30]). One major challenge faced in FL is the potential discrepancies in the local data distributions across distributed clients, which is known as the data heterogeneity issue [33, 36, 45]. Specifically, the private data is collected from different sources with diverse preferences and presents non-independent and identically distributed (*non-iid*) distribution [28, 77]. Such *non-iid* data

discrepancies can lead to inconsistency in the clients’ local objective functions and optimization directions, making the model convergence slow and unstable [18, 30, 31, 40, 67].

To mitigate the negative impact of the data heterogeneity, a mainstream of subsequent efforts delves into introducing a variety of suited signals to regulate the private model, there are mainly two perspectives: i) local model optimization at the client side and ii) global model aggregation at the server side. The former focuses on optimization strategies to make the variance of local updates limited [7, 30]. Another aims to improve the efficacy of global model aggregation [37, 71, 75]. In fact, most of these previous methods force the local models to be consistent to the global model. Although they have a certain effect by reducing gradient inconsistency, the gradually enlarged parameter deviation persists. Hence, we argue that local model overfits the local data distribution, which is magnified under the data heterogeneity and thus hinders the improvement of model’s performance in FL.

Recently, the development of diffusion models (DMs) [4, 12, 38, 47] provides fresh opportunities. The diffusion models have demonstrated remarkable power in generating the diverse and realistic images, showing strong ability to capture intricate details and patterns from underlying data. For instance, with proper guidance, stable diffusion (SD) [47] models can effectively align a text prompt with the corresponding image context, which suggests their potential ability to understand both high-level and low-level contextual visual concepts regarding what an image contains. This semantic generative and visual comprehension capabilities of SD models motivate us to think: *is it possible to exploit the inherent fine-grained visual representation capabilities of diffusion models to promote heterogeneous FL training?*

Taking into account both the effectiveness and efficiency, we revisit the underlying representations in the SD models, which are intermediate feature maps in a diffusion process (e.g., denoise or noise an image) produced by multiple calling a UNet [48]. We argue that diffusion representations are effective steers for FL training: i) extensive general knowledge inherent in diffusion models enhance local semantic diversity in FL; ii) smooth correspondences about semantic objects in diffusion models is a natural guiding signal in FL. Building on these two insights, we first propose **conditional diffusion representations** by imposing various text prompts in the SD model. In this way, each instance is contrastively enhanced with a set of text-driven diffusion representations, capturing rich domain variance. Then, we devise **denoising diffusion representations** from semantic relations between visual and linguistic concepts in the SD model. We extract the feature maps from different hierarchies of the UNet decoder in the SD model’s denoising process, serving as guidance signals to avoid over-optimization in FL local training.

In this paper, we propose a diffusion-inspired **Federated** framework with **Diffusion Representation Collaboration**,

as FedDifRC, to handle the data heterogeneity issue in FL, which consists of two key modules (see Fig. 1): i) **First**, we devise Text-driven Diffusion Contrastive Learning (TDCL), which utilizes conditional diffusion representations to construct inter-contrastive learning [1, 10, 27, 60] in a text-driven diffusion manner (the sample’s embedding is injected as a condition). By maximizing the agreement between the local instance and its corresponding representations, TDCL adaptively captures class-relevant information and semantically meaningful knowledge. This objective encourages sample’s embedding closer to conditional diffusion representations with same semantics and away from other negatives, thus maintaining a clear decision boundary. ii) **Second**, we use the denoising diffusion representations to build a flat and stable convergent target and further propose Noise-driven Diffusion Consistent Restriction (NDCR). Concretely, we extract denoising feature maps of the noisy input sample in the SD model’s backward process, as a regularization term to constrain the optimization region of the local model. The local sample is forced to align the embedding with its denoising representations at the feature space to promote the uniformity for local training. In addition, FedDifRC can be extended to a self-supervised scheme without relying on any labeled data (Sec. 4.3). We also provide a convergence guarantee for FedDifRC under non-convex case (Sec. 4.4). Our main contributions are summarized as follows:

- We explore the possibility of using diffusion models to tackle data heterogeneity in FL and devise the conditional and denoising diffusion representations as effective steers to regulate model training in heterogeneous FL.
- We propose FedDifRC, a diffusion-inspired FL framework to handle data heterogeneity by leveraging the complementary advantages of two key components: i) TDCL facilitates the local model to learn more general class-relevant knowledge; ii) NDCR enforces the uniformity in the feature space for local training.
- We conduct extensive experiments for different FL scenarios (e.g., label shift, domain shift, and long-tailed) and different application scenarios (i.e., intra-domain and cross-domain) to demonstrate the effectiveness of our FedDifRC and the indispensability of each component.

2. Related Work

2.1. Heterogeneous Federated Learning

Federated learning is proposed to address privacy concerns in a distributed learning environment (e.g., Federated Averaging (FedAvg) [35]). Several studies have improved the local update process on the client side or the global aggregation process on the server side to tackle data heterogeneity in FL. The former focuses on local optimization strategies to make the diversity between the client model and the

global model limited in the parameter level [7, 13, 14, 18, 27, 30, 36, 53]. The another branch aims to adopt aggregation mechanisms on the server to alleviate the negative influence of data heterogeneity [24, 44, 62, 64, 71, 75]. Recently, existing FL works that apply diffusion models mainly focus on building synthetic datasets [26, 52, 69, 76]. With the assistance of synthetic datasets, the FL global model can be retrained by this data augmentation scheme to mitigate data heterogeneity. Although these generated data have comparable quality and diversity to client images, the local model may overfit local domain distribution, and the inherent heterogeneity across clients may not have been addressed. In contrast, we focus on how to effectively leverage the fine-grained visual representation from diffusion models to promote a generalizable FL global model.

2.2. Diffusion Model Representations

Recently, diffusion models have shown significant advances in image generation, editing, and stylized [4, 12, 38, 47, 68], suggesting that they contain rich underlying representations to be exploited for different downstream tasks. DIFT [55] is used to extract the diffusion features without explicit supervision. Diffusion Hyperfeatures [32] integrates multi-scale and multi-timesteps diffusion features into feature descriptors. The diffusion representations have shown impressive results on the vision branch, including being testified as certifiable classifiers [3, 25, 65] and semantics correspondence learners [55, 66, 74]. In this paper, we expand the diffusion models to FL and construct the conditional and denoising diffusion representations, offering fruitful class-relevant information and consistent convergence signals.

2.3. Contrastive Learning

Contrastive learning (CL) has been widely applied to self-supervised learning scenarios [1, 8, 10]. Many works are focused on learning the encoder where the embeddings of the same sample are pulled closer and those of different samples are pushed apart [2, 6, 19, 56]. They mainly construct a positive pair and some negative pairs for each data instance and use InfoNCE [39] to contrast positiveness against negativeness. There are some works that incorporate contrastive learning into FL to assist local training to achieve higher model performance [9, 13, 27, 54]. In our work, Text-driven Diffusion Contrastive Learning (TDCL) is devised to promote local model by attracting samples to positive representations while pushing away other negatives.

3. Diffusion Models Help Federated Learning

In this section, we begin with a brief overview of the general FL paradigm and the generative diffusion models (Sec. 3.1). Then, we analyze the effectiveness of diffusion representations and illustrate our core insights (Sec. 3.2). Finally, we

will introduce how to extract the conditional and denoising diffusion representations in Sec. 3.3 and Sec. 3.4.

3.1. Preliminaries and Background

Federated Learning: We focus on the case with K clients holding the heterogeneous data partition $\{\mathcal{D}_1, \mathcal{D}_2, \dots, \mathcal{D}_K\}$ with private dataset $\mathcal{D}_k = \{x_i, y_i\}_{i=1}^{n_k}, y_i \in \{1, \dots, |\mathcal{C}|\}$ for the k -th client, where n_k denotes the local dataset scale. Let n_k^j be the number of samples with label j at client k , and $\mathcal{D}_k^j = \{(x, y) \in \mathcal{D}_k | y = j\}$ denotes the set of samples with label j on the k -th client, so the number of samples in j -th class is $n^j = \sum_{k=1}^K n_k^j$. The objective of the general FL is to learn an optimal global model w across K clients:

$$\min_w \mathcal{L}(w) = \frac{1}{K} \sum_{k=1}^K \frac{n_k}{N} \mathcal{L}_k(w_k; \mathcal{D}_k), \quad (1)$$

where \mathcal{L}_k and w_k are the local loss function and model parameters for the k -th client, respectively. N is the total number of samples among all clients. In the FL training setup, we consider the local model f with parameters $w = \{u, v\}$. It has two modules: i) a feature extractor $h(u)$ with the parameters u maps each sample x_i to a d -dim (default as 512) vector as $z_i = h(u; x_i)$; ii) a classifier $g(v)$ with parameters v maps z_i into a $|\mathcal{C}|$ -dim output logits as $l_i = g(v; z_i)$.

Diffusion Models: A generative diffusion model learns to transform noisy data (typically for a Gaussian distribution) to the high-quality samples of the desired data distribution. Given the image sample x from an underlying distribution $p(x)$, a forward diffusion process as a Markov chain to add random Gaussian noise $\epsilon \sim \mathcal{N}(0, \mathbf{I})$ to the original sample x_0 , and x_t is the noise sample after adding t -steps noise:

$$x_t = \sqrt{1 - \gamma_t} x_{t-1} + \sqrt{\gamma_t} \epsilon_t, \quad t \in \{1, \dots, T\}, \quad (2)$$

where T is the number of diffusion timesteps, $\gamma_t \in (0, 1)$ is a adjustable time variance schedule [12]. By leveraging the additive property of the Gaussian distribution, Eq. (2) can be further reformulated as $x_t = \sqrt{\bar{\alpha}_t} x_0 + \sqrt{1 - \bar{\alpha}_t} \epsilon_t$, where $\alpha_t = 1 - \gamma_t$ and $\bar{\alpha}_t \doteq \prod_{i=1}^t \alpha_i$. On this basis, the image x_0 can be obtained from a random noise $x_t \sim \mathcal{N}(0, \mathbf{I})$ by reversing the above forward diffusion process [12]:

$$x_{t-1} = \frac{1}{\sqrt{\alpha_t}} \left(x_t - \frac{1 - \alpha_t}{\sqrt{1 - \bar{\alpha}_t}} \epsilon_\theta(x_t, t) \right), \quad t \in \{T, \dots, 1\}, \quad (3)$$

where ϵ_θ denotes the denoiser network with the parameters θ to predict noise ϵ , and the denoiser network is usually implemented as a UNet architecture [48]. Further, the denoiser ϵ_θ is optimized using the loss \mathcal{T}_θ as follows:

$$\mathcal{T}_\theta = \mathbb{E}_{\epsilon, x_0, t} [\|\epsilon_\theta(x_t, t) - \epsilon\|_2^2], \quad \epsilon \sim \mathcal{N}(0, \mathbf{I}), \quad (4)$$

where ϵ is the noise in the forward diffusion process, and ϵ_θ is usually implemented as a UNet [48]. Besides, the diffusion model's objective in Eq. (4) can be easily extended to

a conditional diffusion paradigm by adding a condition \mathbf{c} to the ϵ_θ . Thus, the training objective should be modified as:

$$\mathcal{T}_\theta = \mathbb{E}_{\epsilon, x_0, t, \mathbf{c}} [\|\epsilon_\theta(x_t, t, \mathbf{c}) - \epsilon\|_2^2], \quad \epsilon \sim \mathcal{N}(0, \mathbf{I}), \quad (5)$$

with the denoiser $\epsilon_\theta(x_t, t, \mathbf{c})$ in Eq. (5), we can generate data with a specific condition \mathbf{c} by solving a reverse process.

3.2. Motivation and Analysis

The diffusion model is a probabilistic generative model designed for denoising by systematically reversing a progressive noising process, and recent studies [63, 70] have verified that diffusion-based generative models can be effective representation learners. Stable diffusion models are able to weave from scratch with fruitful and innovative depictions of high fidelity and further capture the underlying properties, positions, and correspondences from visual concepts. Such a phenomenon shows that SD models can align a textual prompt with its corresponding image context, demonstrating their potential ability in understanding both high-level (e.g., semantic relations) and low-level (e.g., textures, edge, and structures) visual concepts in an image.

Autoencoders [73, 78] can learn to reconstruct their input at the output and have been one of the dominant approaches for representation learning. We assume a linear autoencoder expressed as $W_a W_b \cdot x + W_c \cdot x$ to imitate UNet [48] used in diffusion models, where $W_a \in \mathbb{R}^{d \times d^*}$, $W_b \in \mathbb{R}^{d^* \times d}$, and $W_c \in \mathbb{R}^{d \times d}$, $d^* < d$. For $x_t = \sqrt{\alpha_t} x_0 + \sqrt{1 - \alpha_t} \epsilon_t$ and we set $\mathbb{E}[x_0] = 0$, thus minimizing the loss \mathcal{T}_θ in Eq. (4) is equivalent to minimize the modified objective \mathcal{T}_θ^* :

$$\begin{aligned} \mathcal{T}_\theta^* &= \mathbb{E}_{\epsilon, x_0, t} [\|\epsilon_\theta(\sqrt{\alpha_t} x_0 + \sqrt{1 - \alpha_t} \epsilon_t) - \epsilon\|_2^2], \\ &\equiv \min \{ \bar{\alpha}_t (W_a W_b + W_c)^\top \Sigma_{x_0} (W_a W_b + W_c) \}, \end{aligned} \quad (6)$$

where Σ_{x_0} means covariance matrix of x_0 . Eq. (6) ensures a meaningful latent space for the diffusion models, similar to the linear autoencoder that encodes data into the principal components space. Therefore, the diffusion training process is equivalent to encourage the disentanglement of the latent representations until good-quality reconstruction is reached.

To validate the representation ability in diffusion models, we use t-SNE [59] to visualize the latent features, shown in Fig. 2, without training on the specific MNIST [23] dataset. Concretely, we use the pre-trained SD model to extract features of the UNet decoder ϵ_θ , T means diffusion time-steps, L means the layer of the UNet decoder ϵ_θ ($L \in \{1, 2, 3, 4\}$). Our results in Fig. 2 indicate that, *even without supervision, diffusion models are able to group input samples* at properly selected time-steps T and layer L . However, when the T or L is too large (e.g., $T = 999$ or $L = 4$), the representations become inseparable, leading to blurred decision boundaries. Furthermore, we apply K-Means clustering (cluster size set as 5) on the latent features from the diffusion UNet decoder and visually examine *whether the diffusion features contain*

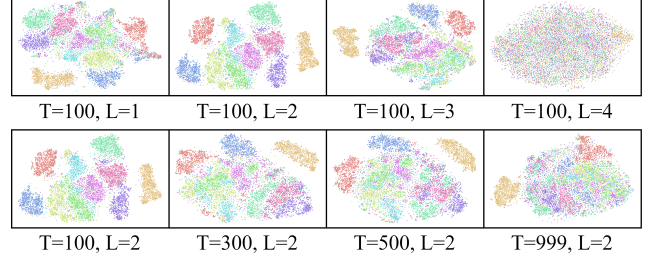


Figure 2. The t-SNE feature visualization on the MNIST dataset from the diffusion UNet decoder, *without training*, where diffusion time-steps $T \in \{100, 300, 500, 999\}$ and layer $L \in \{1, 2, 3, 4\}$.

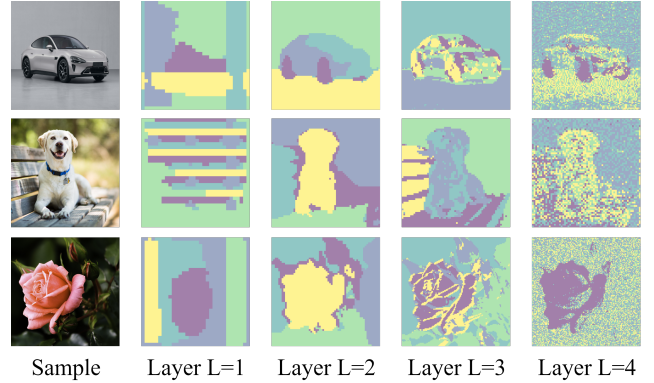


Figure 3. The K-Means clustering feature visualization (each color represents a cluster) from the diffusion UNet decoder’s layers.

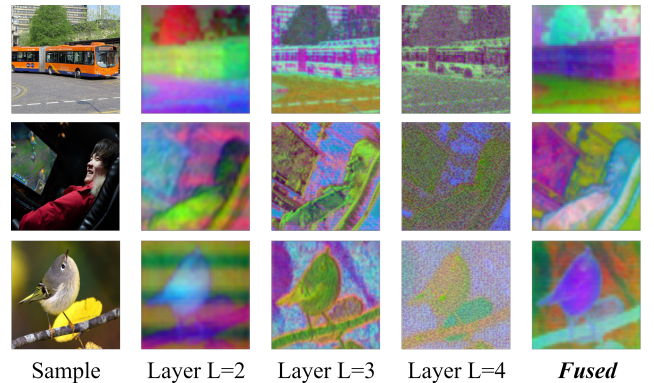


Figure 4. The PCA visualization of early (layer 2), later (layer 4), and *fused features* (see Eq. (8)), where the first three components of PCA-computed serve as color channels for each image.

consistent semantic information. In Fig. 3, different parts of the visual objects are clustered, showing that earlier layers (e.g., $L = 2$) capture coarse yet consistent semantics, while later layers (e.g., $L = 3$) focus on low-level textural details. *Both t-SNE and K-Means observation results motivate us to leverage the fine-grained visual representation capabilities from the SD model to promote heterogeneous FL training.*

3.3. Conditional Diffusion Representations

The key idea of our conditional diffusion representations is based on cognitive diversity of generative diffusion models for different text prompts, via a condition-guided manner. Specifically, for the client k , given an input image x_i of the local dataset $\mathcal{D}_k = \{x_i, y_i\}_{i=1}^{n_k}$, $y_i \in \{1, \dots, |\mathcal{C}|\}$ means the label of x_i , and we let \mathcal{S} represents the set of all class names, so we use \mathcal{S}_{y_i} to denote the class name of the label y_i . From our implementation, the image x_i is fed into the encoder h_k of the local model f_k to obtain the embedding \mathbf{c}_i , then \mathbf{c}_i is treated as a condition and injected into the diffusion model. For a pre-trained SD model, \mathbf{c}_i is further combined with a relevant text prompt $\mathcal{P}_{y_i} = \text{'a photo of a } \mathcal{S}_{y_i} \text{'}$ and sent to the UNet decoder to produce diffusion representations \mathcal{F}_i . Note that since we do not add noise, we simply set the time-steps $T = 0$ of the diffusion process. Typically, the image x_i size is 224×224 , and \mathcal{F}_i contains 4 feature maps, where the L -th layer's feature map $\mathcal{F}_{i(L)}$ has the spatial size $\{7, 14, 28, 28\}$ ($L \in \{1, 2, 3, 4\}$), and $\{1280, 1280, 640, 320\}$ are channels. Formally, conditional diffusion representations \mathcal{F}_i are computed by the ϵ_θ in Eq. (5), image x_i , condition \mathbf{c}_i , text \mathcal{P}_{y_i} :

$$\mathcal{F}_i = \epsilon_\theta(x_i, \tau_i, T = 0, \mathbf{c}_i), \quad \tau_i \leftarrow \varphi(\mathcal{P}_{y_i}), \quad (7)$$

where φ denotes the text encoder of the SD model and τ_i is the text features with the prompt \mathcal{P}_{y_i} . Inspired by the results in Fig. 3, which motivate us to *combine features at different layers of \mathcal{F}_i to capture both semantics and details*. A simple concatenation, however, can lead to an unnecessarily high-dimensional feature ($1280 + 640 + 320 = 2240$). To reduce high dimension, we apply PCA for each layer $L \in \{2, 3, 4\}$ (due to the spatial resolution too low, we do not consider the $L = 1$), and we aggregate them to the same resolution, then we connect them together to obtain the fused features $\tilde{\mathcal{F}}_i$:

$$\tilde{\mathcal{F}}_i = \text{Concat}(\tilde{\mathcal{F}}_{i(L)}), \quad \tilde{\mathcal{F}}_{i(L)} = \text{PCA}(\mathcal{F}_{i(L)}), \quad (8)$$

where $L \in \{2, 3, 4\}$, we perform PCA: i) for $\mathcal{F}_{i(2)}$, we first upsample to the same resolution and apply PCA $\mathbb{R}^{1280 \rightarrow 256}$; ii) for $\mathcal{F}_{i(3)}$ and $\mathcal{F}_{i(4)}$, we apply PCA $\mathbb{R}^{640 \rightarrow 128}$ and PCA $\mathbb{R}^{320 \rightarrow 128}$. Then, we combine them to form the final fused features $\tilde{\mathcal{F}}_i$. As shown in the last column of Fig. 4, *the fused features strike a balance between high-level and low-level visual concepts, focusing on both semantics and textures in the image*. On the example in the second row of Fig. 4, the fused feature yields more accurate matches (e.g., face and computer borders). The comparison results in Table. 2 also confirm this viewpoint. We define $\tilde{\mathcal{F}}_i$ calculated by Eq. (8) as *conditional diffusion representations* of the sample x_i .

3.4. Denoising Diffusion Representations

Although we construct the conditional diffusion representations from the diffusion model's generative feedback, $\tilde{\mathcal{F}}_i$ is still highly variable and depends on the condition generated

by the local model, which can not ensure a consistent stable convergence signal. Based on Eq. (4), we explore the inherent denoising property in diffusion models: SD model has learned extensive general knowledge about identical semantics via large pre-training, reflected in the UNet denoising process. Therefore, we aim to extract the denoising diffusion representations contained in a pre-trained SD model, to align the sample's embedding with the class semantics uniformly in the feature space. Given the image pair $\{x_i, y_i\}$ of k -th client's dataset \mathcal{D}_k , we first perform a forward process to add t time-steps random Gaussian noise on x_i as $\tilde{x}_i^t = \sqrt{\bar{\alpha}_t}x_i + \sqrt{1 - \bar{\alpha}_t}\epsilon_t$, similar to [47], where $\bar{\alpha}_t$ and ϵ are the same as defined in the Eq. (3). Next, we set the text prompt of \tilde{x}_i^t as $\mathcal{P}_{y_i} = \text{'a photo of a } \mathcal{S}_{y_i} \text{'}$ used in the SD model pre-training [47], to avoid destroying correspondence between visual and linguistic concepts, and the \mathcal{S}_{y_i} denotes the class name of the label y_i . Formally, the denoising diffusion representations \mathcal{H}_i of the sample x_i are calculated by the ϵ_θ in Eq. (4), noisy sample \tilde{x}_i^t , text \mathcal{P}_{y_i} :

$$\begin{aligned} \mathcal{H}_i &= \epsilon_\theta(\tilde{x}_i^t, \tau_i, T = t), \quad \tau_i \leftarrow \varphi(\mathcal{P}_{y_i}), \\ \tilde{\mathcal{H}}_i &= \text{Concat}(\tilde{\mathcal{H}}_{i(L)}), \quad \tilde{\mathcal{H}}_{i(L)} = \text{PCA}(\mathcal{H}_{i(L)}), \end{aligned} \quad (9)$$

where φ denotes the text encoder of the SD model and τ_i is the text features of the text prompt \mathcal{P}_{y_i} . We further analyze the effects of the time-steps t in Fig. 6. Then, we combine the features of layers $L \in \{2, 3, 4\}$, like Eq. (8), to obtain fused features \mathcal{H}_i . Intuitively, \mathcal{H}_i is considered as a virtual teacher to calibrate the embedding of x_i at the feature-level. We define the denoising features $\tilde{\mathcal{H}}_i$ calculated by Eq. (9) as *denoising diffusion representations* of the sample x_i .

4. Methodology

Our proposed FedDiffRC leverage conditional and denoising diffusion representations to obtain diverse class-relevant knowledge and consistent convergence signals by two complementary components: Text-driven Diffusion Contrastive Learning in Sec. 4.1 and Noise-driven Diffusion Consistent Restriction in Sec. 4.2. Further, we discuss how to extend FedDiffRC to a self-supervised scheme (Sec. 4.3). Finally, we provide a theoretical analysis of FedDiffRC under non-convex case (Sec. 4.4). Illustration of FedDiffRC in Fig. 5.

4.1. Text-Driven Diffusion Contrasting

Inspired by the success of contrastive learning [1, 10, 27], we deem that a well-generalizable model should provide clear decision boundaries for different classes, instead of biased boundaries limited to the local domain dataset. In this work, based on Sec. 3.3, conditional diffusion representations $\tilde{\mathcal{F}}_i$ of sample $\{x_i, y_i\} \in \mathcal{D}_k$ can be obtained with the condition \mathbf{c}_i and the text prompt $\mathcal{P}_{y_i} = \text{'a photo of a } \mathcal{S}_{y_i} \text{'}$, where \mathcal{S}_{y_i} is the class name of the label y_i . For each sample's embedding $z_i = h_k(x_i) \in \mathbb{R}^d$, we enforce z_i to be

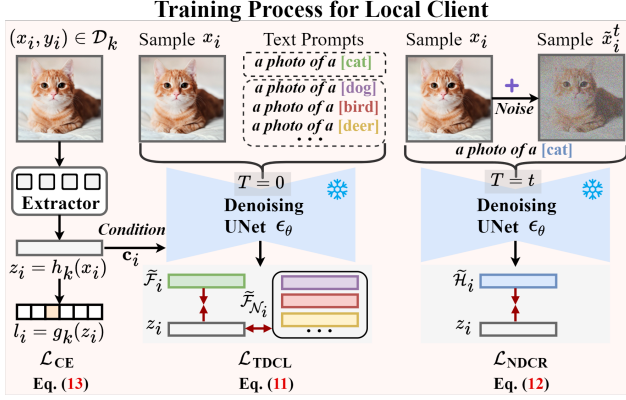


Figure 5. **Illustration of FedDiFRC**, including two complementary modules: TDCL (Sec. 4.1) builds an inter-contrastive learning strategy by conditional diffusion representations (Sec. 3.3), NDCR (Sec. 4.2) designs a consistent regularization penalty via denoising diffusion representations (Sec. 3.4), jointly promoting FL training.

similar to respective positive pair $\tilde{\mathcal{F}}_i$ and dissimilar to negative sample pairs $\tilde{\mathcal{F}}_{N_i}$, where $\tilde{\mathcal{F}}_{N_i}$ means the conditional diffusion representations with the same condition \mathbf{c}_i and the unmatched text prompts $\mathcal{P}_j = \text{'a photo of a } \mathcal{S}_j \text{'}$ ($\mathcal{S}_j \in \mathcal{S}$ and $\mathcal{S}_j \neq \mathcal{S}_{y_i}$). Then, we define the similarity between z_i and $\tilde{\mathcal{F}}_i$ as follows:

$$s(z_i, \tilde{\mathcal{F}}_i) = \frac{z_i \cdot \tilde{\mathcal{F}}_i}{\mathcal{U}(\|z_i\|_2 \times \|\tilde{\mathcal{F}}_i\|_2)}, \quad \mathcal{U} = \frac{1}{n_k} \sum_{m=1}^{n_k} \|z_m - \tilde{\mathcal{F}}_i\|_2, \quad (10)$$

where n_k is total number of samples at client k , \mathcal{U} is a normalization factor for similarity, where we set \mathcal{U} to denote the average distance between $z_m|_{m=1}^{n_k}$ and $\tilde{\mathcal{F}}_i$ on dataset \mathcal{D}_k . Next, we introduce TDCL to quantify and regulate the local model training, which can be formulated as follows:

$$\mathcal{L}_{TDCL} = \log\left(1 + \frac{\sum_{\tilde{\mathcal{F}}_j \in \tilde{\mathcal{F}}_{N_i}} \exp(s(z_i, \tilde{\mathcal{F}}_j)/\tau)}{\exp(s(z_i, \tilde{\mathcal{F}}_i)/\tau)}\right), \quad (11)$$

where τ denotes a temperature parameter to control representation strength [1]. By minimizing Eq. (11), for client k , the local model brings each sample's embedding z_i closer to corresponding positive pair $\tilde{\mathcal{F}}_i$ (\Rightarrow *attractiveness*) and away from other negative pairs $\tilde{\mathcal{F}}_{N_i}$ (\Rightarrow *exclusiveness*), promising satisfying performance in federated learning process.

4.2. Noise-Driven Diffusion Regularization

Despite each local model aligning sample's embedding with conditional diffusion representations by optimizing \mathcal{L}_{TDCL} in Eq. (11). Since conditional diffusion representations are dynamically built from text-driven cross-modal matching and depend on generated condition \mathbf{c}_i at each round, which could not offer a stable convergence direction. Therefore, we aim to leverage denoising diffusion representations ($\tilde{\mathcal{H}}_i$

in Eq. (9)) to devise a consistent regularization penalty, constraining model's optimization region in the feature space. We design Noise-driven Diffusion Consistent Restriction (NDCR) and utilize a regularization term to pull the sample's embedding z_i closer to the respective $\tilde{\mathcal{H}}_i$:

$$\mathcal{L}_{NDCR} = \sum_{q=1}^d (z_{i(q)} - \tilde{\mathcal{H}}_{i(q)})^2, \quad (12)$$

where q indexes the dimension d of the embedding vector. Based on Eq. (12), we expect to align the sample's embedding with the corresponding denoising diffusion representations, enforcing semantics uniformity of the feature space.

Besides, we construct CrossEntropy loss and use the logits output vector $l_i = g(z_i) = f(x_i)$ with the original label y_i to optimize the local discriminative ability for each client. Formally, given the sample pair $\{x_i, y_i\}$ to calculate \mathcal{L}_{CE} :

$$\mathcal{L}_{CE} = -\mathbf{1}_{y_i} \log(\psi(f(x_i))), \quad (13)$$

where ψ denotes the Softmax function, f is the local model with parameters $\{u, v\}$ maps x_i into a $|\mathcal{C}|$ -dim output logits $l_i = f(x_i) = g(h(x_i))$. Finally, for the k -th client, we carry out the following optimization objective in local training:

$$\mathcal{L} = \mathcal{L}_{TDCL}(\text{Eq. (11)}) + \mathcal{L}_{NDCR}(\text{Eq. (12)}) + \mathcal{L}_{CE}. \quad (14)$$

In each communication round, the local model is trained on the private dataset by optimizing \mathcal{L} in Eq. (14), then server collects all local weights to obtain the global weight, which is sent to each participant in the next round. The algorithm of FedDiFRC (overview in Fig. 5) is given in Appendix A.

4.3. Expanding to Self-Supervised Scheme

FedDiFRC can be extended to the self-supervised scheme without relying on any labeled data source. Specifically, for \mathcal{L}_{TDCL} in Eq. (11), we only need to modify text template slightly: i) we set the text prompt $\mathcal{P}_{y_i} = \text{'a photo of a similar object'}$ in Eq. (7) to generate $\tilde{\mathcal{F}}_i$ as the positive pair; ii) then we randomly select from the set of all class names in Tiny-ImageNet [22] to get \mathcal{S}_{N_i} , and set $\mathcal{P}_{y_i} = \text{'a photo of a } \mathcal{S}_{N_i} \text{'}$ to obtain $\tilde{\mathcal{F}}_{N_i}$ as negative pairs. For the \mathcal{L}_{NDCR} in Eq. (12), we set $\mathcal{P}_{y_i} = \text{'a photo of a visual object'}$ in Eq. (9) to get $\tilde{\mathcal{H}}_i$ as consistent signal to align the sample's embedding. Note that it is also possible to use class names of other datasets (e.g., CIFAR100 [21]) to generate $\tilde{\mathcal{F}}_{N_i}$ as negative pairs. By this self-supervised way, the objective term of local training becomes $\mathcal{L}_{TDCL} + \mathcal{L}_{NDCR}$. The results in Table 5 validate the effectiveness of FedDiFRC's self-supervised scheme.

4.4. Convergence Analysis

We proved convergence of FedDiFRC in non-convex case. We denote \mathcal{L} (Eq. (14)) as \mathcal{L}_r with the round r , assumptions (Appendix B.2) are similar to existing works [7, 30, 31, 71].

TDCL	NDCR	CIFAR10 (keep $\rho = 1.0$)				
		NID1 _{0.05}	NID1 _{0.2}	NID1 _{0.5}	NID2	AVG
✓		78.27	84.65	86.11	72.60	80.41
	✓	81.39	86.03	88.16	75.67	82.81
✓	✓	80.35	86.40	87.54	75.33	82.40
		83.14	88.27	89.31	76.45	84.29
TDCL	NDCR	CIFAR10-LT (keep NID1 _{0.2})				
		$\rho = 10$	$\rho = 50$	$\rho = 100$	$\rho = 200$	AVG
✓		75.94	63.25	52.97	49.69	60.46
	✓	76.62	64.66	53.62	50.33	61.31
✓	✓	76.19	64.75	54.39	50.67	61.50
		77.58	65.30	55.01	51.12	62.25

Table 1. Ablation study for two key modules: TDCL and NDCR.

Scenarios	$L = 1$	$L = 2$	$L = 3$	$L = 4$	Fused	Δ
NID1 _{0.05}	80.21	<u>82.60</u>	82.19	81.33	83.14	+ 0.54
NID1 _{0.2}	86.15	87.28	<u>87.81</u>	85.92	88.27	+ 0.46
NID1 _{0.5}	87.10	89.03	88.93	87.17	89.31	+ 0.28
NID2	74.26	<u>75.73</u>	75.61	75.00	76.45	+ 0.72

Table 2. Comparison of features from different layers L and fused features ($L \in \{2, 3, 4\}$) in Eq. (8) and Eq. (9) to obtain $\tilde{\mathcal{F}}_i$ and $\tilde{\mathcal{H}}_i$, **best** in bold and second with underline, Δ means accuracy gap.

Convergence Rate of FedDiffRC: Let the round r from 0 to $R - 1$, given any $\xi > 0$, the \mathcal{L} will converge when,

$$R > \frac{2(\mathcal{L}_0 - \mathcal{L}^*)}{\xi E \eta (2 - L_1 \eta) - \Omega_1 - \Omega_2}, \quad (15)$$

and we can further get the following condition for η ,

$$\eta < \frac{2\xi - 2(|\mathcal{C}| - 1)L_2 B}{L_1(\xi + \sigma^2)}, \quad (16)$$

where $\Omega_1 = 2(|\mathcal{C}| - 1)L_2 E \eta B$, $\Omega_2 = L_1 E \eta^2 \sigma^2$, and \mathcal{L}^* denotes the optimal solution of \mathcal{L} , $\{L_1, L_2, B, \sigma^2\}$ are constants in the assumptions from Appendix B.2, and $|\mathcal{C}|$ as the number of classes, E as local epochs. Eq. (15) and Eq. (16) ensure convergence rate of FedDiffRC, after selecting the number of rounds R and the learning rate η . So the smaller ξ is, the larger R is, which means that the tighter the bound is, the more rounds R is required. *The detailed assumptions and proofs are formally provided in Appendix B.*

5. Experiments

5.1. Experimental Setup

Datasets: We adopt popular benchmark datasets, including CIFAR10 & CIFAR100 [21], TinyImageNet [22]; we build unbalanced versions of these datasets by [16]: CIFAR10-LT & CIFAR100-LT, and TinyImageNet-LT; we use Digits [42] and Office-Caltech [20] for the domain shift task in FL.

Scenarios: i) *label shift*: we consider two *non-iid* settings: NID1 _{α} follows Dirichlet distribution [61], where α denotes the heterogeneity level; NID2 is a more extreme setting consists of 6 biased clients (each has only a single category) and

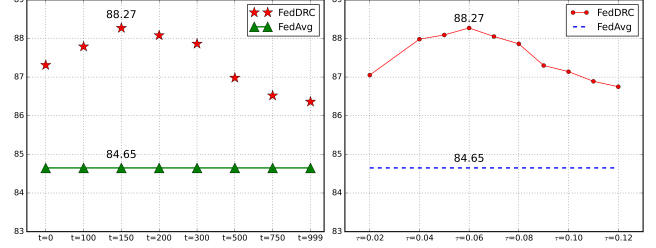


Figure 6. Analysis of FedDiffRC with time-steps t in Eq. (9) (left) and temperature τ in Eq. (11) (right) on CIFAR10 with NID1_{0.2}.

1 unbiased client has all categories. ii) *imbalance shift*: we shape the original dataset into a long-tailed distribution with ρ follow [16], ρ means the ratio between sample sizes of the most frequent and least frequent class, as $\rho = \max_j / \min_j$. iii) *domain shift*: Digits [42] includes 4 domains as MNIST (M), USPS (U), SVHN (SV), SYN (SY) with 10 categories. Office-Caltech [20] also consists 4 domains as Caltech (C), Webcam (W), Amazon (A), DSLR (D) with 10 overlapping categories. We initialize 10 clients and assign them domains randomly: Digits (M: 1, U: 4, SV: 3, SY: 2), Office-Caltech (C: 3, W: 2, A: 2, D: 3). Each client’s dataset is randomly selected from domains (Digits: 10%, Office-Caltech: 20%). **Configurations**: The global rounds R as 100 and clients K as 10, all methods have little or no gain with more rounds R . To facilitate fair comparison, we follow in [27, 30], and use SGD optimizer to update models with a learning rate 0.01, a momentum of 0.9, a batch size of 64, the weight decay of 10^{-5} , and local epochs $E = 10$. We use MobileNetV2 [49] for TinyImageNet, ResNet-10 [15] for others. The dimension d as 512, τ (Eq. (11)) as 0.06, t (Eq. (9)) as 150.

Baselines: We compare our against several SOTA methods: standard-based FedAvg [35], FedProx [30]; contrast-based MOON [27], FedRCL [51]; aggregate-based FedCDA [62], FedDisco [71]; unsupervised FedEMA [79], FedLID [43]; prototype-based FedProto [53], FedNH [72].

5.2. Validation Analysis

We give ablation study in Table. 1: i) TDCL brings significant performance improvements over the baseline, showing that TDCL is able to promote semantic spread-out property; ii) NDCR also yields solid gains, proving the importance of aligning instance embedding via consistency regularization; iii) combining TDCL and NDCR attain better performance, supporting our motivation to unleash meaningful guidance of diffusion representations to promote FL local training.

Then, we prove the advantage of fused features (Eq. (8)). As shown in Table. 2, results on CIFAR10 reveal that fused features capture both semantics and local details, better than features on a single layer L , and if the features with too low resolution ($L=1$) or over-matching ($L=4$) would damage the model’s performance. To explore the influence of different

FL Baselines	CIFAR10			CIFAR100			TinyImageNet			CIFAR10-LT (keep NID1 _{0.2})			
	NID1 _{0.05}	NID1 _{0.2}	NID2	NID1 _{0.05}	NID1 _{0.2}	NID2	NID1 _{0.05}	NID1 _{0.2}	NID2	$\rho = 10$	$\rho = 50$	$\rho = 100$	$\rho = 200$
FedAvg _[AISTAT'17]	78.27	84.65	72.60	55.97	60.08	50.56	40.41	42.84	35.15	75.94	63.25	52.97	49.69
FedProx _[MLSys'20]	78.42	84.59	72.81	56.27	60.21	50.29	40.20	42.16	35.62	76.02	63.43	52.86	49.10
MOON _[CVPR'21]	80.79	86.10	73.35	56.79	61.48	51.81	40.79	43.63	36.11	75.73	63.80	53.17	49.31
FedProto _[AAAI'22]	77.86	83.90	70.84	54.48	59.26	48.60	39.29	41.02	34.68	74.31	62.23	50.37	47.26
FedNH _[AAAI'23]	80.25	85.82	73.65	56.68	61.45	51.31	40.25	43.30	36.21	76.15	63.36	52.49	48.92
FedDisco _[ICML'23]	81.35	86.63	74.72	57.34	61.79	52.05	40.83	43.92	37.69	76.27	64.40	53.33	49.75
FedCDA _[ICLR'24]	81.70	86.89	75.07	57.76	<u>62.17</u>	52.35	41.18	44.09	38.24	<u>76.45</u>	64.30	<u>53.85</u>	<u>50.08</u>
FedRCL _[CVPR'24]	<u>82.02</u>	<u>87.11</u>	<u>75.13</u>	<u>57.98</u>	62.05	<u>52.49</u>	<u>41.33</u>	<u>44.21</u>	<u>38.86</u>	76.34	64.17	53.41	49.91
FedDifRC	83.14	88.27	76.45	59.22	63.32	53.87	42.63	45.28	40.05	77.58	65.30	55.01	51.12

Table 3. Comparison results on several settings (label shift and imbalance shift) and datasets, the **best** in bold and second with underline.

FL Baselines	Office-Caltech				
	Caltech	Webcam	Amazon	DSLR	AVG
FedDisco _[ICML'23]	62.39	45.95	77.31	45.20	57.71
FedCDA _[ICLR'24]	62.25	46.53	76.58	46.14	<u>57.87</u>
FedRCL _[CVPR'24]	60.13	42.76	75.60	43.77	55.56
FedDifRC	63.32	50.19	78.67	48.12	60.08

Table 4. Comparison results on Office-Caltech with domain shift.

FL Baselines	Clients	CIFAR100			
		NID1 _{0.05}	NID1 _{0.2}	NID1 _{0.5}	NID2
FedEMA _[ICLR'22]	$K = 10$	26.90	29.41	30.64	21.52
FedLID _[ICCV'23]	$K = 10$	28.84	30.43	31.22	23.65
FedDifRC	$K = 10$	30.61	31.45	32.30	25.73

Table 5. Comparison results on self-supervised setting (Sec. 4.3).

FL Baselines	CIFAR10			CIFAR10-LT (NID1 _{0.2})		
	NID1 _{0.05}	NID1 _{0.2}	NID2	$\rho = 10$	$\rho = 50$	$\rho = 100$
FedDDA _[PRCV'23]	82.05	86.94	74.49	76.31	63.95	53.15
FedDISC _[AAAI'24]	82.33	87.15	75.42	76.60	64.23	54.07
FedRCL ($\diamond + \dagger$)	82.30 [◇] /86.95 [†]	87.25 [◇] /86.16 [†]	75.37 [◇] /73.85 [†]	76.50 [◇] /76.12 [†]	64.26 [◇] /62.91 [†]	53.65 [◇] /52.20 [†]
FedRCL ($\diamond + \ddagger$)	81.52	86.48	74.35	76.22	63.69	52.93
FedDifRC	83.14	88.27	76.45	77.58	65.30	55.01

Table 6. More comparison results on CIFAR10 and CIFAR10-LT.

FL Baselines	HAM10000 [57]			EuroSAT [41]		
	NID1 _{0.2}	NID1 _{0.5}	NID2	NID1 _{0.2}	NID1 _{0.5}	NID2
FedDisco _[ICML'23]	50.26	53.68	44.63	78.76	82.36	70.34
FedCDA _[ICLR'24]	51.65	54.05	45.16	<u>80.45</u>	83.38	<u>71.10</u>
FedRCL _[CVPR'24]	<u>52.21</u>	<u>54.20</u>	<u>45.48</u>	79.80	<u>83.69</u>	70.73
FedDifRC	53.79	55.60	47.17	82.49	86.05	73.14

Table 7. Comparison results on the HAM10000 and EuroSAT.

time-steps t (Eq. (9)), we conduct experiments on CIFAR10 with NID1_{0.2} in Fig. 6 left, we add different amount of noise to get \tilde{x}_t^t in Eq. (9). We find that FedDifRC is robust to the choice of $t \in [100, 300]$ ($t=150$ achieves the highest value). With the increase of t , more and more details are removed and semantic-level features are preserved, but when t is too

Pre-trained Models	CIFAR10			CIFAR10-LT (NID1 _{0.2})		
	NID1 _{0.05}	NID1 _{0.2}	NID2	$\rho = 10$	$\rho = 50$	$\rho = 100$
CLIP-ViT-B/16 [46]	79.72	84.91	73.97	74.89	62.44	50.87
MAE-ViT-B/16 [11]	80.74	85.38	73.24	75.45	63.27	52.55
DINO-ViT-B/16 [34]	80.57	86.14	74.16	75.25	62.70	51.92
FedDifRC	83.14	88.27	76.45	77.58	65.30	55.01

Table 8. Experiments on aligning features of pre-trained models.

large, the object structure is distorted in the sample, making poor performance. In Fig. 6 right, we show the results with different τ in Eq. (11), which reveals that FedDifRC is not sensitive to the $\tau \in [0.04, 0.08]$, indicating the effectiveness of \mathcal{U} (Eq. (10)), to balance relative distances among different samples. The accuracy no longer increases after $\tau=0.06$. Extra results of t and τ are provided in Appendix C.2.5.

5.3. Evaluation Results

The results on different settings (NID1, NID2, ρ) in Table. 3, FedDifRC consistently outperforms these counterparts, it confirms that FedDifRC effectively leverages the inherent fine-grained visual representation capabilities of diffusion models to promote heterogeneous FL training. The results of Office-Caltech with domain shift are shown in Table. 4, indicating that FedDifRC can acquire well-generalizable property in the feature space. With self-supervised scenario, in Table. 5, our FedDifRC achieves excellent performance by leveraging the visual perception capability of diffusion models, without requiring any labeled data. The results with the imbalance shift on CIFAR100-LT and TinyImageNet-LT datasets, and the results with domain shift on the Digits, are given in Appendix C.2.2 and C.2.3. We also compare the convergence rate of FedDifRC and baselines, shown in Appendix C.2.4, indicating the superiority of FedDifRC in dealing with heterogeneous FL scenarios and the efficiency for FL model training. The ablation study on the number of clients K and local epochs E for FedDifRC are provided in Appendix C.2.7 and C.2.8. Since our FedDifRC is built on the SD model, we also investigate how the SD model’s weights would affect the performance of FedDifRC. In our

previous experiments, SD-1.5 as basic SD model, we then compare different versions (e.g., SD-1.4, SD-2.0) of the SD model on CIFAR10, and the results are shown in Appendix C.2.9 (e.g., SD-1.4 get 83.09% and 88.23% of NID_{10.05} and NID_{10.2}). Our initial purpose is not to generate the image, different SD model versions have almost little difference.

To further elaborate on the core idea of FedDiffRC, i.e., we study how to fully leverage the fine-grained visual representation capabilities from diffusion models (e.g., condense visual concepts and their relations) to boost the performance of heterogeneous FL, we set the following experiments:

i) *To ensure a fair comparison*, we also compare diffusion-based FL methods FedDISC [69] and FedDDA [76], which build synthetic datasets to enhance performance. Moreover, we generate data for each client (same amount) by the SD model as \diamond , and align SD features (the image is fed directly into the SD model) by L2 loss as \dagger . Table. 6 shows that directly matching SD features may even hurt the performance, which further illustrates the superiority of our FedDiffRC.

ii) *We focus on visual perception ability of diffusion models to understand an image (e.g., textures and structures) rather than pre-trained prior knowledge*. We conduct experiments on medical and remote sensing datasets HAM10000 [57] and EuroSAT [41], which are not crossed in SD pre-training dataset LAION-5B [50]. Results of intra-domain (Table. 3) and cross-domain (Table. 7) datasets show that the success of FedDiffRC is based on the fine-grained visual representation rather than the large prior knowledge in SD model.

iii) *The SD model can implicitly provide both high-level and low-level visual concepts of semantic objects, while foundation models focus more on sparse visual matching*. Due to the natural heterogeneity in FL, simply aligning the features of foundation models may lead to local overfitting. We align FedAvg features with foundation model by L2 loss, shown in Table. 8, which show that FedDiffRC can capture underlying properties and correspondences of visual objects. Our TDCL and NDCR modules unlock the semantic-generative and fine-grained representation capabilities in the SD model to promote model training in heterogeneous FL.

6. Conclusion

In this paper, we aim to exploit the fine-grained visual representation capabilities of diffusion models to handle data heterogeneity in FL. We propose a novel diffusion-inspired FL framework FedDiffRC to regulate local training via denoising and conditional diffusion representations. By leveraging complementary strength of TDCL and NDCR, FedDiffRC achieves superior performance in heterogeneous FL.

Acknowledgment

This work is supported by the scholarship from the China Scholarship Council (CSC) while the first author pursues

his PhD degree at the University of Wollongong. This work was also partially supported by Australian Research Council Linkage Project LP210300009 and LP230100083.

A. Algorithm Pseudocode Flow

In this section, we describe the pseudocode of FedDiffRC in Algorithm 1: i) Client Process: for each client k , loss as $\mathcal{L} = \mathcal{L}_{TDCL} + \mathcal{L}_{NDCR} + \mathcal{L}_{CE}$ (Eq. 14); ii) Server Process: aggregate all local models (same as FedAvg [35]).

Algorithm 1 Pseudocode of FedDiffRC.

```

RunServer( $w_k$ ): /* Global Server Process */
1: Initialized global rounds  $R$ , number of clients  $K$ , number of classes  $|\mathcal{C}|$ ,  $k$ -th client's dataset  $\mathcal{D}_k(x, y)$ , client local model  $w_k$ , and global model  $w_g$ 
2: Note: Conditional Diffusion Representations  $\tilde{\mathcal{F}}_i$  (Eq.8), Denoising Diffusion Representations  $\tilde{\mathcal{H}}_i$  (Eq.9)
3: for each round  $r = 1, 2, \dots, R$  do
4:    $A_r \leftarrow$  (server selects a random subset of  $K$  clients)
5:   for each client  $k \in A_r$  in parallel do
6:      $w_k \leftarrow \text{RunClient}(w_g)$ 
7:   end for
8:   // global aggregation
9:    $w_g \leftarrow \sum_{k=1}^{|A_r|} \frac{n_k}{N} w_k$ 
10: end for

RunClient( $w_g$ ): /* Local Client Process */
11: Initialized local epochs  $E$ , size of samples  $n_k$ , learning rate  $\eta$ , local model  $f(w_k)$ , client's dataset  $\mathcal{D}_k$ 
12: for each local epoch  $e = 1, 2, \dots, E$  do
13:   for each batch  $b \in$  client dataset  $\mathcal{D}_k$  do
14:      $\mathcal{L}_{CE} = \sum_{i \in b} -1_{y_i} \log(\psi(f(w_k; x_i)))$ 
15:     // Text-driven Diffusion Contrastive Learning
16:      $\mathcal{L}_{TDCL} \leftarrow \{z_i, \tilde{\mathcal{F}}_i, \tilde{\mathcal{F}}_{N_i}\}$  (Eq.11 in Sec.4.1)
17:     // Noise-driven Diffusion Consistent Restriction
18:      $\mathcal{L}_{NDCR} \leftarrow \{z_i, \tilde{\mathcal{H}}_i\}$  (Eq.12 in Sec.4.2)
19:     // training loss objective
20:      $\mathcal{L} = \mathcal{L}_{CE} + \mathcal{L}_{TDCL} + \mathcal{L}_{NDCR}$ 
21:     // model update by the SGD optimizer
22:      $w_k \leftarrow w_k - \eta \nabla \mathcal{L}(w_k; b)$ 
23:   end for
24: end for
25: return  $w_k$ 

```

B. Theoretical Analysis for FedDiffRC

In this section, we herein provide insights into the convergence analysis for FedDiffRC under the non-convex case. This theoretical analysis of FedDiffRC is grounded in four standard assumptions prevalent in the field of FL, which are similarly invoked across various scholarly works [7, 30, 31, 71]. The detailed description of notations in Sec. B.1, standard assumptions in Sec. B.2, and our proofs in Sec. B.3.

B.1. Preliminaries

Here, we introduce some additional variables to better represent the FL training process and model updates from a mathematical perspective. For the k -th client, based on Sec. 3.1, define the local model $f(x) = g(h(x))$ with parameters w , where h is the feature extractor maps each sample x to a d -dim feature vector $z = h(x)$, and g is the classifier maps vector z into a $|\mathcal{C}|$ -dim output logits $l = g(z)$. In addition, $\mathcal{D}_k = \{x_i, y_i\}_{i=1}^{n_k}$ is the training dataset for the k -th client, n_k is the number of total samples, the label y_i of single sample belongs to one of $|\mathcal{C}|$ categories and is expressed as $y_i \in \{1, \dots, |\mathcal{C}|\}$. In FedDifRC process, for the client k , given the sample pair $\{x_i, y_i\} \in \mathcal{D}_k$, based on Sec. 3.3 and Sec. 3.4, we can obtain conditional diffusion representations $\tilde{\mathcal{F}}_i$ (Eq. 8), and denoising diffusion representations $\tilde{\mathcal{H}}_i$ (Eq. 9). We denote the loss objective function $\mathcal{L} = \mathcal{L}_{TDCL}$ (Eq. 11) + \mathcal{L}_{NDCR} (Eq. 12) + \mathcal{L}_{CE} (Eq. 13) defined as \mathcal{L}_r with a subscript indicating the round r of the global iterations in our FedDifRC process.

We express $\mathbf{e} \in \{1, 2, \dots, E\}$ as the local iteration step, r as the global round, E as the local epochs, $rE + \mathbf{e}$ refers to the \mathbf{e} -th local update in round $r + 1$, $rE + 1$ denotes the time between r -th global aggregation at the server and starting the model update on round $r + 1$ at the local client. Therefore, if the step is at $rE + 1$ of local client iterations, the local model is the same as rE .

B.2. Assumptions

Let $h_{k,r}(u_{k,r}) \in \mathbb{R}^d$ be the feature extractor, $g_{k,r}(v_{k,r}) \in \mathbb{R}^{|\mathcal{C}|}$ be the classifier to calculate logits, $w_{k,r} = \{u_{k,r}, v_{k,r}\}$ denotes parameters of the client model $f_{k,r}$, and $\mathcal{L}_{k,r}$ means the objective function, at the k -th client on the round r . Our theoretical analysis of FedDifRC is based on the following four standard assumptions in FL:

Assumption 1 (Smoothness). *For each objective function \mathcal{L} is L_1 -Lipschitz smooth, which suggests the gradient of objective function \mathcal{L} is L_1 -Lipschitz continuous:*

$$\begin{aligned} \|\nabla \mathcal{L}_{k,r_1} - \nabla \mathcal{L}_{k,r_2}\|_2 &\leq L_1 \|w_{k,r_1} - w_{k,r_2}\|_2, \\ \forall r_1, r_2 > 0, \quad k &\in \{1, \dots, K\}, \end{aligned} \quad (17)$$

since the smoothness depends on the derivative of the differentiable function, it also indicates the following quadratic bound ($L_1 > 0$):

$$\begin{aligned} \mathcal{L}_{k,r_1} - \mathcal{L}_{k,r_2} &\leq (\nabla \mathcal{L}_{k,r_2})^\top (w_{k,r_1} - w_{k,r_2}) \\ &\quad + \frac{L_1}{2} \|w_{k,r_1} - w_{k,r_2}\|_2^2. \end{aligned} \quad (18)$$

Assumption 2 (Unbiased Gradient and Bounded Variance). *For each client, the stochastic gradient is unbiased (ζ is the sample of the client's dataset), so the unbiased gradient is*

expressed as follows:

$$\begin{aligned} \mathbb{E}_\zeta[\nabla \mathcal{L}(w_{k,r}, \zeta)] &= \nabla \mathcal{L}(w_{k,r}) = \nabla \mathcal{L}_r, \\ \forall k &\in \{1, \dots, K\}, \quad r > 0, \end{aligned} \quad (19)$$

and has bounded variance:

$$\begin{aligned} \mathbb{E}_\zeta[\|\nabla \mathcal{L}(w_{k,r}, \zeta) - \nabla \mathcal{L}(w_{k,r})\|_2^2] &\leq \sigma^2, \\ \forall k &\in \{1, \dots, K\}, \quad \sigma^2 \geq 0. \end{aligned} \quad (20)$$

Assumption 3 (Bounded Dissimilarity of Stochastic Gradients). *For each objective function \mathcal{L} , there exists constant B such that the stochastic gradient is bounded:*

$$\begin{aligned} \mathbb{E}_\zeta[\|\nabla \mathcal{L}(w_{k,r}, \zeta)\|_2] &\leq B, \\ \forall k &\in \{1, \dots, K\}, \quad B > 0, \quad r > 0. \end{aligned} \quad (21)$$

Assumption 4 (Continuity). *For each real-valued function $h(u)$ is L_2 -Lipschitz continuous:*

$$\begin{aligned} \|h_{k,r_1}(u_{k,r_1}) - h_{k,r_2}(u_{k,r_2})\| &\leq L_2 \|u_{k,r_1} - u_{k,r_2}\|_2, \\ \forall r_1, r_2 > 0, \quad k &\in \{1, \dots, K\}. \end{aligned} \quad (22)$$

B.3. Completing Proofs

In this subsection, based on the above four assumptions, we present the following three theorems and prove them:

Theorem 1 (Deviation bound of the objective function \mathcal{L}). *Under the assumptions, after every communication round, objective function \mathcal{L} of an arbitrary client will be bounded,*

$$\begin{aligned} \mathbb{E}[\mathcal{L}_{(r+1)E}] &\leq \mathcal{L}_{rE} - \left(\eta - \frac{L_1 \eta^2}{2}\right) EB^2 + \frac{L_1 E \eta^2}{2} \sigma^2 \\ &\quad + (|\mathcal{C}| - 1) L_2 E \eta B, \end{aligned} \quad (23)$$

where η is the learning rate, $|\mathcal{C}|$ is the number of classes, $\{L_1, L_2, B, \sigma^2\}$ are the constants in the above assumptions. Theorem 1 indicates that \mathcal{L}_r decreases as round r increases, and the convergence of our FedDifRC can be guaranteed by choosing an appropriate η .

Theorem 2 (Non-convex convergence of FedDifRC). *Under the assumptions, the objective function \mathcal{L} of an arbitrary client decreases monotonically as the round increases with the following condition,*

$$\eta_{\mathbf{e}} < \frac{2B^2 - 2(|\mathcal{C}| - 1)L_2 B}{L_1(\sigma^2 + B^2)}, \quad \mathbf{e} \in \{1, 2, \dots, E - 1\}. \quad (24)$$

Theorem 3 (Non-convex convergence rate of FedDifRC). *Let the assumptions hold, the round r from 0 to $R - 1$, given any $\xi > 0$, the objective function \mathcal{L} will converge when,*

$$R > \frac{2(\mathcal{L}_0 - \mathcal{L}^*)}{\xi E \eta (2 - L_1 \eta) - \Omega_1 - \Omega_2}, \quad (25)$$

and we can further get the following condition for η ,

$$\eta < \frac{2\xi - 2(|\mathcal{C}| - 1)L_2B}{L_1(\xi + \sigma^2)}, \quad (26)$$

where $\Omega_1 = 2(|\mathcal{C}| - 1)L_2E\eta B$, $\Omega_2 = L_1E\eta^2\sigma^2$, and \mathcal{L}^* denotes the optimal solution of \mathcal{L} , i.e., $\mathcal{L}^* = \min\{\mathcal{L}\}$.

Theorem 1 indicates the deviation bound of the objective function \mathcal{L} for an arbitrary client after each round, and the convergence can be guaranteed by choosing appropriate η . Theorem 2 is to ensure the expected deviation of \mathcal{L} to be negative, so FedDifRC's objective function converges, which can guide the choice of appropriate values for the learning rate η to guarantee the convergence. Theorem 3 provides the convergence rate of FedDifRC: the smaller ξ is, the larger R is, which means that the tighter the bound is, the more communication rounds R is required.

B.3.1. Completing the Proof of Theorem 1

Proof of Theorem 1. The Theorem 1 is applicable to an arbitrary client in FedDifRC, therefore we omit the client's notation k , and define the gradient descent as $w_{r+1} = w_r - \eta \nabla \mathcal{L}_r(w_r) = w_r - \eta \theta_r$, then we can get:

$$\begin{aligned} \mathcal{L}_{rE+2} &\stackrel{(i)}{\leq} \mathcal{L}_{rE+1} + (\nabla \mathcal{L}_{rE+1})^\top (w_{rE+2} - w_{rE+1}) \\ &\quad + \frac{L_1}{2} \|w_{rE+2} - w_{rE+1}\|_2^2 \\ &= \mathcal{L}_{rE+1} - \eta (\nabla \mathcal{L}_{rE+1})^\top \theta_{rE+1} + \frac{L_1}{2} \|\eta \theta_{rE+1}\|_2^2, \end{aligned} \quad (27)$$

where (i) from L_1 -Lipschitz quadratic bound of the above Assumption 1. We perform the expectation on both sides:

$$\begin{aligned} \mathbb{E}[\mathcal{L}_{rE+2}] &\leq \mathcal{L}_{rE+1} - \eta \mathbb{E}[(\nabla \mathcal{L}_{rE+1})^\top \theta_{rE+1}] \\ &\quad + \frac{L_1}{2} \eta^2 \mathbb{E}[\|\theta_{rE+1}\|_2^2] \\ &\stackrel{(i)}{=} \mathcal{L}_{rE+1} - \eta \mathbb{E}[\|\nabla \mathcal{L}_{rE+1}\|_2^2] \\ &\quad + \frac{L_1}{2} \eta^2 \mathbb{E}[\|\theta_{rE+1}\|_2^2] \\ &\stackrel{(ii)}{\leq} \mathcal{L}_{rE+1} - \eta \mathbb{E}[\|\nabla \mathcal{L}_{rE+1}\|_2^2] + \\ &\quad \frac{L_1}{2} \eta^2 (\mathbb{E}^2[\|\nabla \mathcal{L}_{rE+1}\|_2] + \text{Variance}[\|\theta_{rE+1}\|_2]) \\ &= \mathcal{L}_{rE+1} - \eta \|\nabla \mathcal{L}_{rE+1}\|_2^2 + \frac{L_1}{2} \eta^2 (\|\nabla \mathcal{L}_{rE+1}\|_2^2 \\ &\quad + \text{Variance}[\|\theta_{rE+1}\|_2]) \\ &= \mathcal{L}_{rE+1} + (\frac{L_1}{2} \eta^2 - \eta) \|\nabla \mathcal{L}_{rE+1}\|_2^2 \\ &\quad + \frac{L_1}{2} \eta^2 \text{Variance}[\|\theta_{rE+1}\|_2] \\ &\stackrel{(iii)}{\leq} \mathcal{L}_{rE+1} + (\frac{L_1}{2} \eta^2 - \eta) \|\nabla \mathcal{L}_{rE+1}\|_2^2 + \frac{L_1}{2} \eta^2 \sigma^2, \end{aligned} \quad (28)$$

where (i) from the stochastic gradient is unbiased in Eq. 19 of the Assumption 2; (ii) from the formula: $\text{Variance}(x) = \mathbb{E}[x^2] - \mathbb{E}^2[x]$; (iii) from the Eq. 20 of the Assumption 2. Then, $rE + 1$ means the time between the server and client, and $rE + 2$ means the first step, we telescope E steps on both sides of the above equation:

$$\begin{aligned} \mathbb{E}[\mathcal{L}_{(r+1)E}] &\leq \mathcal{L}_{rE+1} + (\frac{L_1}{2} \eta^2 - \eta) \sum_{e=1}^{E-1} \|\nabla \mathcal{L}_{rE+e}\|_2^2 \\ &\quad + \frac{L_1}{2} E \eta^2 \sigma^2, \end{aligned} \quad (29)$$

and then we consider the relationship between \mathcal{L}_{rE+1} and \mathcal{L}_{rE} , that is, given the any sample ζ , we consider the relationship between $\mathcal{L}_{(r+1)E+1}$ and $\mathcal{L}_{(r+1)E}$ as follows:

$$\begin{aligned} \mathcal{L}_{(r+1)E+1} &= \mathcal{L}_{(r+1)E} + (\mathcal{L}_{CE,(r+1)E+1} + \mathcal{L}_{TDCL,(r+1)E+1} \\ &\quad + \mathcal{L}_{NDCR,(r+1)E+1}) - \mathcal{L}_{(r+1)E} \\ &= \mathcal{L}_{(r+1)E} + \mathcal{L}_{TDCL,(r+1)E+1} - \mathcal{L}_{TDCL,(r+1)E} \\ &\stackrel{(i)}{\leq} \mathcal{L}_{(r+1)E} + \log(\sum_{\tilde{\mathcal{F}}_j \in \tilde{\mathcal{F}}_{\mathcal{N}_i,(r+1)E+1}} \exp(s(\zeta, \tilde{\mathcal{F}}_j))) \\ &\quad - \log(\sum_{\tilde{\mathcal{F}}_j \in \tilde{\mathcal{F}}_{\mathcal{N}_i,(r+1)E}} \exp(s(\zeta, \tilde{\mathcal{F}}_j))) \\ &\stackrel{(ii)}{\leq} \mathcal{L}_{(r+1)E} + \sum_{\tilde{\mathcal{F}}_j \in \tilde{\mathcal{F}}_{\mathcal{N}_i}} (\|h_{k,(r+1)E}(\zeta)\|_2 \\ &\quad - \|h_{k,rE}(\zeta)\|_2) \\ &\stackrel{(iii)}{\leq} \mathcal{L}_{(r+1)E} + \sum_{\tilde{\mathcal{F}}_j \in \tilde{\mathcal{F}}_{\mathcal{N}_i}} (\|h_{k,(r+1)E}(\zeta) - h_{k,rE}(\zeta)\|_2) \\ &\stackrel{(iv)}{\leq} \mathcal{L}_{(r+1)E} + (|\mathcal{C}| - 1) \sum_{k=1}^K \frac{n_k}{N} (\|h_{k,(r+1)E}(\zeta) - h_{k,rE}(\zeta)\|_2) \\ &\stackrel{(v)}{\leq} \mathcal{L}_{(r+1)E} + (|\mathcal{C}| - 1) L_2 \sum_{k=1}^K \frac{n_k}{N} (\|u_{k,(r+1)E} - u_{k,rE}\|_2) \\ &\stackrel{(vi)}{\leq} \mathcal{L}_{(r+1)E} + (|\mathcal{C}| - 1) L_2 \sum_{k=1}^K \frac{n_k}{N} (\|w_{k,(r+1)E} - w_{k,rE}\|_2) \\ &= \mathcal{L}_{(r+1)E} + (|\mathcal{C}| - 1) L_2 \sum_{k=1}^K \frac{n_k}{N} \|\eta \sum_{e=1}^{E-1} \theta_{k,rE+e}\|_2 \\ &= \mathcal{L}_{(r+1)E} + (|\mathcal{C}| - 1) L_2 \eta \sum_{k=1}^K \frac{n_k}{N} \|\sum_{e=1}^{E-1} \theta_{k,rE+e}\|_2 \\ &\stackrel{(vii)}{\leq} \mathcal{L}_{(r+1)E} + (|\mathcal{C}| - 1) L_2 \eta \sum_{k=1}^K \frac{n_k}{N} \sum_{e=1}^{E-1} \|\theta_{k,rE+e}\|_2, \end{aligned} \quad (30)$$

where (i) from the objective function in Paper Eq. 11; (ii) based on Paper Eq. 10: $s(z, \tilde{\mathcal{F}}_j) = (\frac{1}{\mathcal{U}} \cdot \frac{1}{\|z\|_2} \cdot \frac{\tilde{\mathcal{F}}_j}{\|\tilde{\mathcal{F}}_j\|_2})z \leq z$,

then we take expectation to get $\mathbb{E}[s(z, \tilde{\mathcal{F}}_j)] \leq \|z\|_2$, and $z = h(\zeta)$; (iii) from the formula as: $\|x\|_2 - \|y\|_2 \leq \|x - y\|_2$; (iv) details from the Sec. 3.1 and Sec. 3.3, and ζ is the sample of the client dataset; (v) from the Eq. 22 of the Assumption 4; (vi) from the fact that u is a subset of $w = \{u, v\}$; (vii) from the formula as $\|\sum x\|_2 \leq \sum \|x\|_2$. Then, we perform the expectation on both sides of Eq. 30:

$$\begin{aligned} \mathbb{E}[\mathcal{L}_{(r+1)E+1}] &\leq \mathcal{L}_{(r+1)E} + \\ &(|\mathcal{C}| - 1)L_2\eta \sum_{k=1}^K \frac{n_k}{N} \sum_{e=1}^{E-1} \mathbb{E}[\|\theta_{k,rE+e}\|_2] \\ &\stackrel{(i)}{\leq} \mathcal{L}_{(r+1)E} + (|\mathcal{C}| - 1)L_2\eta EB, \end{aligned} \quad (31)$$

where (i) from Assumption 3, and we can easily get:

$$\mathbb{E}[\mathcal{L}_{rE+1}] \leq \mathcal{L}_{rE} + (|\mathcal{C}| - 1)L_2\eta EB, \quad (32)$$

then, based on Eq. 29 and Eq. 32, we can get:

$$\begin{aligned} \mathbb{E}[\mathcal{L}_{(r+1)E}] &\leq \mathcal{L}_{rE} + (|\mathcal{C}| - 1)L_2\eta EB + \frac{L_1}{2}E\eta^2\sigma^2 \\ &+ \left(\frac{L_1}{2}\eta^2 - \eta\right) \sum_{e=1}^{E-1} \|\nabla \mathcal{L}_{rE+e}\|_2^2 \\ &\stackrel{(i)}{\leq} \mathcal{L}_{rE} - \left(\eta - \frac{L_1}{2}\eta^2\right)EB^2 + \frac{L_1E\eta^2}{2}\sigma^2 \\ &+ (|\mathcal{C}| - 1)L_2\eta EB, \end{aligned} \quad (33)$$

where (i) from the Eq. 21 of the Assumption 3.

Theorem 1 indicates the deviation bound of the loss objective function for an arbitrary client after each communication round. Convergence can be guaranteed when there is a certain expected one-round decrease, which can be achieved by choosing an appropriate η . We have completed the proof of Theorem 1 for FedDifRC. \square

B.3.2. Completing the Proof of Theorem 2

Proof of Theorem 2. Based on Theorem 1, we can get:

$$\begin{aligned} \mathbb{E}[\mathcal{L}_{(r+1)E}] - \mathcal{L}_{rE} &\leq -\left(\eta - \frac{L_1}{2}\eta^2\right)EB^2 + \frac{L_1E\eta^2}{2}\sigma^2 \\ &+ (|\mathcal{C}| - 1)L_2\eta EB. \end{aligned} \quad (34)$$

Then, to ensure the right side of the above equation $T_1 = -\left(\eta - \frac{L_1}{2}\eta^2\right)EB^2 + \frac{L_1E\eta^2}{2}\sigma^2 + (|\mathcal{C}| - 1)L_2\eta EB \leq 0$, we can easily get the following condition for η :

$$\eta_e < \frac{2B^2 - 2(|\mathcal{C}| - 1)L_2B}{L_1(\sigma^2 + B^2)}, \quad e \in \{1, 2, \dots, E-1\}. \quad (35)$$

So, the convergence of objective function \mathcal{L} in FedDifRC holds as round r increases and the above limitation of the learning rate η in Eq. 35. We have completed the proof of Theorem 2 for FedDifRC. \square

B.3.3. Completing the Proof of Theorem 3

Proof of Theorem 3. Based on the Eq. 33, we can get:

$$\begin{aligned} \mathbb{E}[\mathcal{L}_{(r+1)E}] &\leq \mathcal{L}_{rE} + (|\mathcal{C}| - 1)L_2E\eta B + \frac{L_1}{2}E\eta^2\sigma^2 \\ &+ \left(\frac{L_1}{2}\eta^2 - \eta\right) \sum_{e=1}^{E-1} \|\nabla \mathcal{L}_{rE+e}\|_2^2. \end{aligned} \quad (36)$$

Further, we can get the following equation by Eq. 36:

$$\begin{aligned} \sum_{e=1}^{E-1} \|\nabla \mathcal{L}_{rE+e}\|_2^2 &\leq \frac{2(|\mathcal{C}| - 1)L_2E\eta B}{2\eta - L_1\eta^2} + \\ &\frac{2(\mathcal{L}_{rE} - \mathbb{E}[\mathcal{L}_{(r+1)E}]) + L_1E\eta^2\sigma^2}{2\eta - L_1\eta^2}. \end{aligned} \quad (37)$$

Let the round r from 0 to $R-1$, step e from 1 to E , we can easily get the following equation:

$$\begin{aligned} \frac{1}{RE} \sum_{r=0}^{R-1} \sum_{e=1}^{E-1} \mathbb{E}[\|\nabla \mathcal{L}_{rE+e}\|_2^2] &\leq \frac{2 \sum_{r=0}^{R-1} (\mathcal{L}_{rE} - \mathbb{E}[\mathcal{L}_{(r+1)E}])}{RE(2\eta - L_1\eta^2)} \\ &+ \frac{2(|\mathcal{C}| - 1)L_2\eta B}{2\eta - L_1\eta^2} \\ &+ \frac{L_1\eta^2\sigma^2}{2\eta - L_1\eta^2}, \end{aligned} \quad (38)$$

and then, given any $\xi > 0$, \mathcal{L} and R receive the limitation:

$$\begin{aligned} \xi &> \frac{\frac{2}{RE} \sum_{r=0}^{R-1} (\mathcal{L}_{rE} - \mathbb{E}[\mathcal{L}_{(r+1)E}])}{2\eta - L_1\eta^2} + \\ &\frac{2(|\mathcal{C}| - 1)L_2\eta B + L_1\eta^2\sigma^2}{2\eta - L_1\eta^2}, \end{aligned} \quad (39)$$

then we can easily get the following condition for R :

$$R > \frac{2(\mathcal{L}_0 - \mathcal{L}^*)}{\underbrace{\xi E \eta (2 - L_1 \eta) - \Omega_1 - \Omega_2}_{T_2}}, \quad (40)$$

where

$$\Omega_1 = 2(|\mathcal{C}| - 1)L_2E\eta B, \quad (41)$$

and

$$\Omega_2 = L_1E\eta^2\sigma^2, \quad (42)$$

where \mathcal{L}^* denotes the optimal solution of objective \mathcal{L} , and $\sum_{r=0}^{R-1} (\mathcal{L}_{rE} - \mathbb{E}[\mathcal{L}_{(r+1)E}]) = \mathcal{L}_0 - \mathcal{L}_1 + \mathcal{L}_1 - \mathcal{L}_2 + \dots + \mathcal{L}_{R-1} - \mathcal{L}_R = \mathcal{L}_0 - \mathcal{L}_R \leq \mathcal{L}_0 - \mathcal{L}^*$. Then, the denominator of the above equation in Eq. 40 should satisfy $T_2 > 0$, so we can easily obtain the following condition for η :

$$\eta < \frac{2\xi - 2(|\mathcal{C}| - 1)L_2B}{L_1(\xi + \sigma^2)}. \quad (43)$$

Theorem 3 provides convergence rate of FedDifRC, which can confine the gradients of the objective function \mathcal{L} to any bound, denoted as ξ , after carefully selecting the number of rounds R in Eq. 40 and hyperparameters η in Eq. 43. The smaller ξ is, the larger R is, which means that the tighter the bound is, the more communication rounds R is required. We have completed the proof of Theorem 3 for FedDifRC. \square

C. Experimental Details and Extra Results

In this section, we additionally provide more experimental results. All experiments are conducted on a 64-bit Ubuntu-18.04 system with two NVIDIA RTX A5000 GPUs. Note that all results reported are the average of three repeating runs with a standard deviation of different random seeds.

C.1. Experimental Details

For all experiments, we run $R = 100$ rounds and set the number of clients as $K = 10$. We conduct local training for $E = 10$ epochs in each communication round using the SGD optimizer with a learning rate of 0.01, a momentum of 0.9, a batch size of 64, and a weight decay set $1e - 5$. We apply the data augmentation of [5] in TinyImageNet dataset experiments. The regularization coefficient of FedProx [30] μ is tuned across $\{10^{-4}, 10^{-3}, 10^{-2}, 10^{-1}\}$ and is selected to be $\mu = 10^{-3}$; the regularization coefficient of MOON [27] μ is tuned across $\{0.1, 1.0, 3.0, 5.0, 6.0\}$ and is selected to be $\mu = 1.0$; the regularization coefficient of FedProto [53] λ is tuned across $\{1.0, 2.0, 3.0, 4.0\}$ and is selected to be $\lambda = 1.0$; the smoothing parameter of FedNH [72] ρ is tuned across $\{0.1, 0.2, 0.5, 0.7, 0.8, 0.9\}$ and is selected to be $\rho = 0.7$; the regularization coefficient of FedRCL [51] λ is tuned across $\{0.2, 0.4, 0.6, 0.8\}$ and is selected to be $\lambda = 0.6$, and divergence penalty β is tuned across $\{0.5, 1.0, 2.0, 3.0, 4.0\}$ and is selected to be $\beta = 1.0$; the temperature parameter of FedLID [43] \mathcal{T} is tuned across $\{0.02, 0.04, 0.06, 0.08, 0.1\}$ and is selected to be $\mathcal{T} = 0.04$. We take out a 20% subset of the training set for validation and return the validation set back to the training set, and re-train the model after selecting the optimal hyperparameters $\tau = 0.06$ and $t = 150$.

Datasets: i) CIFAR10 [21] and CIFAR100 [21] both have 50,000 training samples and 10,000 test samples, and each sample is a 32×32 color image, CIFAR10 has all 10 categories and CIFAR100 has 100 categories; ii) CIFAR10-LT and CIFAR100-LT, we follow [16] to shape the original balanced CIFAR10 and CIFAR100 into long-tailed data distribution with ρ respectively. The sample size and the number of categories have not changed; iii) TinyImageNet [22] contains 200 classes, with 100,000 training samples and 10,000 testing samples, and each image’s size is 64×64 . We follow from [16] to generate the unbalanced version TinyImageNet-LT of the TinyImageNet with long-tailed

level ρ ; iv) The Digits [42] includes 4 domains as MNIST (M), USPS (U), SVHN (SV), SYN (SY) with the 10 categories; v) Office-Caltech [20] also consists 4 domains as Caltech (C), Webcam (W), Amazon (A), DSLR (D) with 10 categories.

Models: i) ResNet-10 [15]: we follow [15] setup for image classification task. ResNet-10 is stacked by multiple bottleneck building blocks and each bottleneck building block is made of three convolutional layers, with the kernel size 1, 3, and 1, we use a stack of $6n$ layers with 3×3 convolutions, the sizes of the feature maps are $\{32, 16, 8\}$ respectively, with $2n$ layers for each feature map size; ii) MobileNetV2 [49] is a lightweight, efficient deep neural network architecture designed specifically for mobile and embedded vision applications. MobileNetV2 improves upon its predecessor by significantly reducing the number of parameters and computations while maintaining or even improving performance. We use the ResNet-10 [15] for CIFAR10, CIFAR100, Digits, and Office-Caltech, MobileNetV2 [49] for Tiny-ImageNet.

C.2. Extra Results

C.2.1. Comparison results with label shift

The comparison results for FedDifRC and compared FL baselines with different heterogeneity settings (NID1 $_{\alpha}$ and NID2) are shown in Table. 9. We observe that FedDifRC universally outperforms other methods, which implies that FedDifRC can effectively exploit meaningful knowledge from diffusion models to boost model training. Experiments show that: i) FedDifRC consistently outperforms others in various *non-iid* settings, showing that FedDifRC is robust to different heterogeneity levels, even in the more difficult NID2 setting; ii) based on the TDCL and NDCR modules, FedDifRC potentially enhances the semantic diversity and uniformity of local model training under heterogeneous FL, yields improvements over baselines.

C.2.2. Comparison results with imbalance shift

The comparison results for FedDifRC and compared FL baselines with different imbalanced levels ρ are shown in Table 10. We observe that: i) FedDifRC achieves the significantly better results on imbalance settings with long-tail distribution, which confirms the benefit of diffusion representations to regulate local training, even in the scenario of the global-level class imbalance; ii) FedDifRC alleviates the negative impact of long-tailed distribution by leveraging meaningful guidance from pre-trained diffusion models.

C.2.3. Comparison results with domain shift

The comparison results of Digits and Office-Caltech with domain shift are shown in Table. 11, where different clients are equipped with the data samples from different domains: Digits (MNIST: 1, USPS: 4, SVHN: 3, SYN: 2) and Office-Caltech (Caltech: 3, Webcam: 2, Amazon: 2, DSLR: 3).

FL Baselines	CIFAR10				CIFAR100				TinyImageNet			
	NID1 _{0.05}	NID1 _{0.2}	NID1 _{0.5}	NID2	NID1 _{0.05}	NID1 _{0.2}	NID1 _{0.5}	NID2	NID1 _{0.05}	NID1 _{0.2}	NID1 _{0.5}	NID2
FedAvg _[AISTAT'17]	78.27	84.65	86.11	72.60	55.97	60.08	62.48	50.56	40.41	42.84	43.88	35.15
FedProx _[MLSys'20]	78.42	84.59	86.16	72.81	56.27	60.21	62.53	50.29	40.20	42.16	43.56	35.62
MOON _[CVPR'21]	80.79	86.10	87.49	73.35	56.79	61.48	63.38	51.81	40.79	43.63	44.32	36.11
FedProto _[AAAI'22]	77.86	83.90	85.41	70.84	54.48	59.26	61.19	48.60	39.29	41.02	42.27	34.68
FedNH _[AAAI'23]	80.25	85.82	87.03	73.65	56.68	61.45	63.10	51.31	40.25	43.30	44.53	36.21
FedDisco _[ICML'23]	81.35	86.63	87.92	74.72	57.34	61.79	63.62	52.05	40.83	43.92	45.13	37.69
FedCDA _[ICLR'24]	81.70	86.89	88.20	75.07	57.76	<u>62.17</u>	63.95	52.35	41.18	44.09	<u>45.34</u>	38.24
FedRCL _[CVPR'24]	<u>82.02</u>	<u>87.11</u>	<u>88.28</u>	<u>75.13</u>	<u>57.98</u>	62.05	<u>64.21</u>	<u>52.49</u>	<u>41.33</u>	<u>44.21</u>	45.18	<u>38.86</u>
FedDifRC	83.14	88.27	89.31	76.45	59.22	63.32	65.12	53.87	42.63	45.28	46.24	40.05

Table 9. Comparison results on CIFAR10, CIFAR100, and TinyImageNet datasets with label shift, **best** in bold and second with underline.

FL Baselines	CIFAR10-LT (keep NID1 _{0.2})				CIFAR100-LT (keep NID1 _{0.2})				TinyImageNet-LT (keep NID1 _{0.2})			
	$\rho = 10$	$\rho = 50$	$\rho = 100$	$\rho = 200$	$\rho = 10$	$\rho = 50$	$\rho = 100$	$\rho = 200$	$\rho = 10$	$\rho = 50$	$\rho = 100$	$\rho = 200$
FedAvg _[AISTAT'17]	75.94	63.25	52.97	49.69	50.83	42.60	32.19	30.25	33.85	24.10	20.92	19.18
FedProx _[MLSys'20]	76.02	63.43	52.86	49.10	50.45	42.21	32.28	30.23	33.89	24.13	20.61	18.91
MOON _[CVPR'21]	75.73	63.80	53.17	49.31	51.18	43.14	32.90	30.72	34.25	24.73	21.09	19.16
FedProto _[AAAI'22]	74.31	62.23	50.37	47.26	48.65	41.20	31.38	28.61	32.40	22.32	19.77	17.73
FedNH _[AAAI'23]	76.15	63.36	52.49	48.92	51.72	43.24	33.15	30.81	34.37	25.07	21.68	19.53
FedDisco _[ICML'23]	76.27	<u>64.40</u>	53.33	49.75	52.14	43.45	33.41	31.03	35.27	25.79	21.99	19.75
FedCDA _[ICLR'24]	<u>76.45</u>	64.30	<u>53.85</u>	<u>50.08</u>	<u>52.21</u>	43.70	33.74	<u>31.27</u>	<u>35.55</u>	<u>25.89</u>	<u>22.05</u>	<u>19.95</u>
FedRCL _[CVPR'24]	76.34	64.17	53.41	49.91	51.98	<u>43.93</u>	<u>33.83</u>	30.92	35.13	25.40	21.87	19.60
FedDifRC	77.58	65.30	55.01	51.12	53.13	44.87	35.08	32.47	36.69	26.96	23.12	21.27

Table 10. Comparison results on CIFAR10-LT, CIFAR100-LT, and TinyImageNet-LT datasets with imbalance shift, ρ means the long-tailed ratio between sample sizes of the most frequent and least frequent class (*i.e.*, $\rho = \max_j \{n_j\} / \min_j \{n_j\}$).

FL Baselines	Digits [42]				
	MNIST	USPS	SVHN	SYN	AVG
FedAvg _[AISTAT'17]	98.01	90.85	76.56	55.14	80.14
FedProx _[MLSys'20]	98.11	90.24	77.09	56.50	80.48
FedDisco _[ICML'23]	98.14	91.80	78.03	57.48	81.35
FedCDA _[ICLR'24]	97.86	92.44	80.35	57.85	<u>82.13</u>
FedRCL _[CVPR'24]	98.30	92.16	76.90	54.22	80.39
FedDifRC	98.35	93.40	81.54	60.32	83.40

FL Baselines	Office-Caltech [20]				
	Caltech	Webcam	Amazon	DSLR	AVG
FedAvg _[AISTAT'17]	60.15	45.86	75.44	38.13	54.89
FedProx _[MLSys'20]	60.21	43.62	76.59	38.30	54.68
FedDisco _[ICML'23]	62.39	45.95	77.31	45.20	57.71
FedCDA _[ICLR'24]	62.25	46.53	76.58	46.14	<u>57.87</u>
FedRCL _[CVPR'24]	60.13	42.76	75.60	43.77	55.56
FedDifRC	63.32	50.19	78.67	48.12	60.08

Table 11. Comparison results on Digits [42] and Office-Caltech [20] datasets with domain shift setting (different clients are equipped with the data samples from different domains).

Each client’s dataset is randomly selected from the domains (Digits: 10%, Office-Caltech: 20%). The experiments show that FedDifRC performs significantly better than other FL baselines, which confirms that our proposed FedDifRC

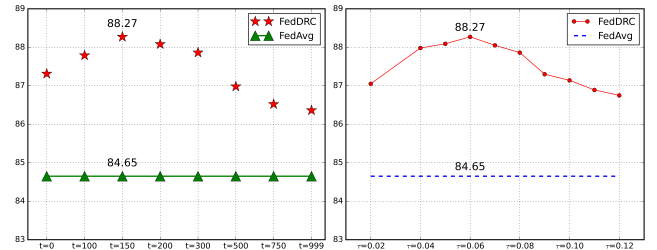


Figure 7. Analysis of FedDifRC with time-steps t in Eq. 9 (left) and temperature τ in Eq. 11 (right) on CIFAR10 with NID10.2.

can acquire well-generalizable property of the feature space during the heterogeneous FL training with domain shift.

C.2.4. Comparison results of convergence rates

The comparison results of convergence rates on CIFAR10, CIFAR100, and TinyImageNet are shown in Table 12. Our FedDifRC required fewer rounds to converge compared with other baselines and achieved a higher final accuracy, showing the superiority of FedDifRC in dealing with *non-iid* data and its robust stability, which also indicates that FedDifRC helps to promote training generalizability and efficiency of heterogeneous FL in the feature space.

FL Baselines	CIFAR10 (keep NID _{10,2})				CIFAR100 (keep NID _{10,2})				TinyImageNet (keep NID _{10,2})			
	$R_{20\%}$	$R_{40\%}$	$R_{80\%}$	ACC	$R_{20\%}$	$R_{40\%}$	$R_{60\%}$	ACC	$R_{20\%}$	$R_{30\%}$	$R_{40\%}$	ACC
FedAvg _[AISTAT'17]	5	15	52	84.65	9	33	80	60.08	16	35	58	42.84
FedProx _[MLSys'20]	5	13	49	84.59	9	32	76	60.21	16	33	56	42.16
MOON _[CVPR'21]	3	8	42	86.10	6	25	69	61.48	10	29	48	43.63
FedProto _[AAAI'22]	7	20	66	83.90	17	46	-	59.26	25	49	71	41.02
FedNH _[AAAI'23]	6	12	45	85.82	10	30	76	61.45	16	30	52	43.30
FedDisco _[ICML'23]	3	8	39	86.63	6	25	65	61.79	9	28	50	43.92
FedCDA _[ICLR'24]	3	10	40	86.89	7	22	57	<u>62.17</u>	9	25	50	44.09
FedRCL _[CVPR'24]	3	7	36	<u>87.11</u>	6	23	55	62.05	8	26	45	<u>44.21</u>
FedDi fRC	3	5	27	88.27	5	17	43	63.32	6	18	32	45.28

Table 12. Comparison results of convergence rates on CIFAR10, CIFAR100, and TinyImageNet. The R_{acc} columns denote the minimum number of rounds required to reach acc of the test accuracy, and the ACC columns show the final test accuracy.

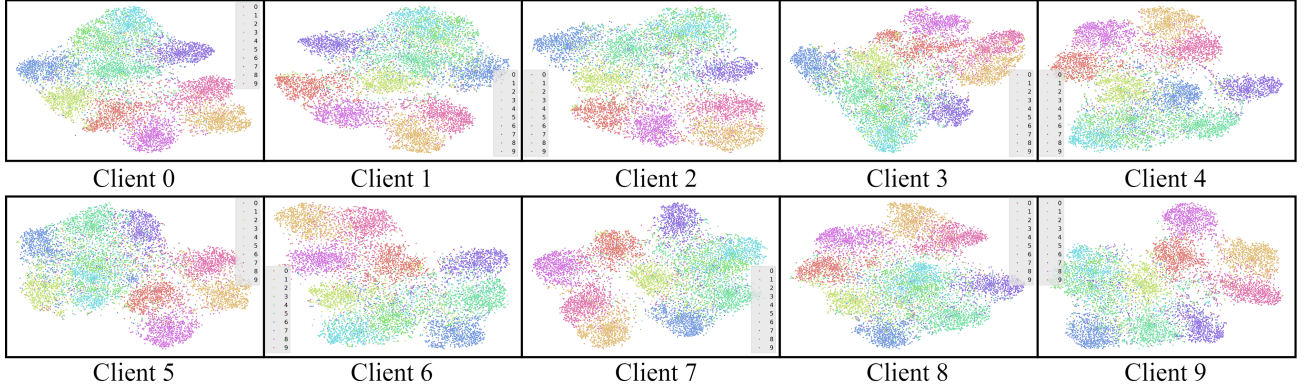


Figure 8. The t-SNE visualization of FedDi fRC on local clients under the CIFAR10 dataset (NID_{10,2}, $\rho = 10$).

Datasets	different time-steps t						
	$t=100$	$t=150$	$t=200$	$t=300$	$t=500$	$t=750$	$t=999$
CIFAR10	87.87	88.27	<u>88.08</u>	87.91	86.98	86.52	86.29
CIFAR100	<u>62.93</u>	63.32	62.90	62.78	61.59	61.34	61.15
TinyImageNet	44.86	45.28	<u>45.20</u>	44.79	43.25	43.16	43.02

Table 13. Results of time-steps t for different datasets with NID_{10,2}.

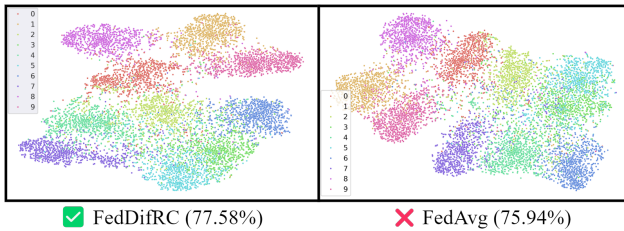


Figure 9. The t-SNE visualization of FedDi fRC and FedAvg on the global model under the CIFAR10 dataset (NID_{10,2}, $\rho = 10$).

C.2.5. Effects of time-steps t and temperature τ

To explore the influence of time-steps t in Eq. 9 and temperature τ in Eq. 11, we conduct experiments on CIFAR10 with NID_{10,2}, shown in Fig. 7. In Fig. 7 left, we add different amounts of noise to get \tilde{x}_i^t in Eq. 9, FedDi fRC is robust to the choice of $t \in [100, 300]$ ($t = 150$ achieves the highest value). With the increase of time-steps t , more and more details are removed and semantic-level features are preserved, but when t is too large, the object structure is distorted in the sample, making poor performance. In Fig. 7 right, we show the results with different τ in Eq. 11, which reveals that FedDi fRC is not sensitive to the $\tau \in [0.04, 0.08]$, indicating the effectiveness of \mathcal{U} in Eq. 10, to balance relative distances among different samples. The accuracy no longer increases after $\tau = 0.06$. In Table. 13, we provide results of the time-steps t for different datasets with NID_{10,2} setting. Based on these results, to prevent the redundancy of adjusting parameters, we thus set $t = 150$ and $\tau = 0.06$ in our experiments as default values.

FL Baselines	$K = 10$	$K = 20$	$K = 30$	$K = 50$	$K = 100$
FedAvg _[AISTAT'17]	42.84	40.27	38.02	35.27	32.85
FedDisco _[ICML'23]	43.92	41.75	38.81	37.30	34.74
FedCDA _[ICLR'24]	44.09	42.50	39.47	37.58	35.22
FedRCL _[CVPR'24]	44.21	42.68	39.96	38.14	35.17
FedDifRC	45.28	43.92	41.64	40.81	37.50

Table 14. Ablation study of the number of clients K on TinyImageNet with NID1_{0.2}.

FL Baselines	$E = 1$	$E = 5$	$E = 10$	$E = 15$	$E = 20$
FedAvg _[AISTAT'17]	35.88	42.02	42.84	41.75	39.30
FedDisco _[ICML'23]	36.91	42.69	43.92	42.03	40.85
FedCDA _[ICLR'24]	37.24	43.25	44.09	42.32	41.54
FedRCL _[CVPR'24]	37.65	43.39	44.21	42.63	41.76
FedDifRC	39.18	44.61	45.28	43.87	43.14

Table 15. Ablation study of the number of local epochs E on TinyImageNet with NID1_{0.2}.

C.2.6. Visualization analysis via t-SNE

In Fig. 8, we compare representations of local models under the NID1_{0.2} with $\rho = 10$ setting on CIFAR10 via t-SNE [58] visualization. We can observe that FedDifRC forces each local model to learn more clearer classification boundaries by both TDCL and NDCR modules, thus promoting a more generalizable FL global model. We also visualize the global model of FedDifRC and FedAvg, shown in Fig. 9.

C.2.7. Ablation study on the number of clients K

The comparison results of clients K on TinyImageNet are shown in Table. 14. We can observe that FedDifRC brings significant performance gains even under more challenging settings with more clients. These experiments demonstrate the potential of our FedDifRC to be applied to real-world settings with massive numbers of clients and random client participation. Moreover, these results under random client participation show that the improvements from FedDifRC are robust to such uncertainties.

C.2.8. Ablation study on the number of local epochs E

We ablate on the number of local epochs per communication round. We set the number of local epochs E to be in the set $\{1, 5, 10, 15, 20\}$. The comparison results of local epochs E on TinyImageNet are shown in Table. 15, in which one observes that with increasing E , FedAvg performance first increases and then decreases. This is because when E is too small, the local training cannot converge properly in each communication round. On the other hand, when E is too large, the model parameters of local clients might be driven to be too far from the global optimum. Nevertheless, FedDifRC consistently improves over the baselines across different choices of local epochs E .

SD versions	CIFAR10					
	NID1 _{0.05}	NID1 _{0.2}	NID1 _{0.5}	NID2	AVG	Δ
SD-1.4	83.09	88.23	89.25	76.33	84.23	- 0.06
SD-1.5	83.14	88.27	89.31	76.45	84.29	-
SD-2.0	<u>83.12</u>	88.30	<u>89.29</u>	<u>76.40</u>	84.27	- 0.02

Table 16. Effects of different SD model weights for FedDifRC, and Δ means the average accuracy gap with SD-1.5.

C.2.9. Effects of different SD model weights

Since FedDifRC is built on the SD model, we also investigate how the SD model’s weights would affect the performance of FedDifRC. In our previous experiments, we set the released 1-5 version of the stable diffusion model [47] (SD-1.5) as the basic SD model. We compare different versions of the SD model weights, and the results are shown in Table. 16. Compared with the SD-1.5 version, the SD-2.0 version adopts a larger model architecture and parameters. Our initial purpose is not to generate the image, different versions of the SD model have almost little difference. The results also show that the success of FedDifRC is based on the fine-grained visual representation capabilities from the SD model rather than the large capacity model architecture and prior knowledge.

C.2.10. Efficiency for FedDifRC

In our FedDifRC process, we only introduced the frozen UNet decoder of the SD model in the model training, with no additional overhead during testing. During the training process, we stored the diffusion representations to further reduce the memory overhead. For example, training on the CIFAR10 dataset: FLOPs (FedAvg 132.9G, FedDifRC 187.6G), Time (FedAvg 155.25m, FedDifRC 230.08m). During the testing process, since no additional model is introduced, FedDifRC shares the same number of parameters as other FL baselines.

References

- [1] Ting Chen, Simon Kornblith, Mohammad Norouzi, and Geoffrey Hinton. A simple framework for contrastive learning of visual representations. In *ICML*, pages 1597–1607, 2020. 2, 3, 5, 6
- [2] Ching-Yao Chuang, Joshua Robinson, Yen-Chen Lin, Antonio Torralba, et al. Debaised contrastive learning. In *NeurIPS*, pages 8765–8775, 2020. 3
- [3] Kevin Clark and Priyank Jaini. Text-to-image diffusion models are zero shot classifiers. In *NeurIPS*, 2023. 3
- [4] Florinel-Alin Croitoru, Vlad Hondru, Radu Tudor Ionescu, and Mubarak Shah. Diffusion models in vision: A survey. *IEEE TPAMI*, 45(9):10850–10869, 2023. 2, 3
- [5] Ekin D. Cubuk, Barret Zoph, Dandelion Mane, Vijay Vasudevan, et al. Autoaugment: Learning augmentation strategies from data. In *CVPR*, pages 113–123, 2019. 13

- [6] Jiequan Cui, Zhisheng Zhong, Shu Liu, Bei Yu, et al. Parametric contrastive learning. In *ICCV*, pages 715–724, 2021. 3
- [7] Liang Gao, Huazhu Fu, Li Li, Yingwen Chen, et al. Feddc: Federated learning with non-iid data via local drift decoupling and correction. In *CVPR*, pages 10112–10121, 2022. 2, 3, 6, 9
- [8] Jie Gui, Tuo Chen, Jing Zhang, Qiong Cao, et al. A survey on self-supervised learning: Algorithms, applications, and future trends. *IEEE TPAMI*, 46(12):9052–9071, 2024. 3
- [9] Sungwon Han, Sungwon Park, Fangzhao Wu, Sundong Kim, et al. Fedx: Unsupervised federated learning with cross knowledge distillation. In *ECCV*, pages 691–707, 2022. 3
- [10] Kaiming He, Haoqi Fan, Yuxin Wu, Saining Xie, et al. Momentum contrast for unsupervised visual representation learning. In *CVPR*, pages 9729–9738, 2020. 2, 3, 5
- [11] Kaiming He, Xinlei Chen, Saining Xie, Yanghao Li, et al. Masked autoencoders are scalable vision learners. In *CVPR*, pages 16000–16009, 2022. 8
- [12] Jonathan Ho, Ajay Jain, and Pieter Abbeel. Denoising diffusion probabilistic models. In *NeurIPS*, pages 6840–6851, 2020. 2, 3
- [13] Wenke Huang, Mang Ye, and Bo Du. Learn from others and be yourself in heterogeneous federated learning. In *CVPR*, pages 10143–10153, 2022. 3
- [14] Wenke Huang, Mang Ye, Zekun Shi, He Li, and Bo Du. Rethinking federated learning with domain shift: A prototype view. In *CVPR*, pages 16312–16322, 2023. 3
- [15] Cheng Ju, Aurélien Bibaut, and Mark van der Laan. The relative performance of ensemble methods with deep convolutional neural networks for image classification. *Journal of Applied Statistics*, 45:2800–2818, 2018. 7, 13
- [16] Cao Kaidi, Colin Wei, Adrien Gaidon, Nikos Archiga, et al. Learning imbalanced datasets with label-distribution-aware margin loss. In *NeurIPS*, 2019. 7, 13
- [17] Peter Kairouz, H Brendan McMahan, Brendan Avent, Aurélien Bellet, et al. Advances and open problems in federated learning. *Foundations and Trends in Machine Learning*, 14(1):1–210, 2021. 1
- [18] Sai Praneeth Karimireddy, Satyen Kale, Mehryar Mohri, Sashank Reddi, et al. Scaffold: Stochastic controlled averaging for federated learning. In *ICML*, pages 5132–5143, 2020. 2, 3
- [19] Prannay Khosla, Piotr Teterwak, Chen Wang, Aaron Sarna, et al. Supervised contrastive learning. In *NeurIPS*, pages 18661–18673, 2020. 3
- [20] Boqing Kong, Yuan Shi, Fei Sha, and Kristen Grauman. Geodesic flow kernel for unsupervised domain adaptation. In *CVPR*, pages 2066–2073, 2012. 7, 13, 14
- [21] Alex Krizhevsky and Geoffrey Hinton. Learning multiple layers of features from tiny images. In *Technical report, University of Toronto*, 2009. 6, 7, 13
- [22] Ya Le and Xuan Yang. Tiny imagenet visual recognition challenge. *CS 231N*, 7, 2015. 6, 7, 13
- [23] Yann LeCun, Léon Bottou, Yoshua Bengio, and Patrick Haffner. Gradient-based learning applied to document recognition. *Proceedings of the IEEE*, 86(11):2278–2324, 1998. 4
- [24] Sunwoo Lee, Tuo Zhang, and A Salman Avestimehr. Layer-wise adaptive model aggregation for scalable federated learning. In *AAAI*, pages 8491–8499, 2023. 3
- [25] Alexander C Li, Mihir Prabhudesai, Shivam Duggal, Ellis Brown, et al. Your diffusion model is secretly a zero-shot classifier. In *ICCV*, pages 2206–2217, 2023. 3
- [26] Daixun Li, Weiyang Xie, Zixuan Wang, Yibing Lu, et al. Feddiff: Diffusion model driven federated learning for multi-modal and multi-clients. *IEEE TCSVT*, 34(10):10353–10367, 2024. 3
- [27] Qinbin Li, Bingsheng He, and Dawn Song. Model-contrastive federated learning. In *CVPR*, pages 10713–10722, 2021. 2, 3, 5, 7, 13
- [28] Qinbin Li, Yiqun Diao, Quan Chen, and Bingsheng He. Federated learning on non-iid data silos: An experimental study. In *ICDE*, pages 965–978, 2022. 1
- [29] Tian Li, Anit Kumar Sahu, Ameet Talwalkar, and Virginia Smith. Federated learning: Challenges, methods, and future directions. *IEEE SPM*, 37(3):50–60, 2020. 1
- [30] Tian Li, Anit Kumar Sahu, Manzil Zaheer, Maziar Sanjabi, et al. Federated optimization in heterogeneous networks. *MLSys*, 2:429–450, 2020. 1, 2, 3, 6, 7, 9, 13
- [31] Xiang Li, Kaixuan Huang, Wenhao Yang, Shusen Wang, et al. On the convergence of fedavg on non-iid data. In *ICLR*, 2020. 2, 6, 9
- [32] Grace Luo, Lisa Dunlap, Dong Huk Park, Aleksander Holynski, et al. Diffusion hyperfeatures: Searching through time and space for semantic correspondence. In *NeurIPS*, 2023. 3
- [33] Mi Luo, Fei Chen, Dapeng Hu, Yifan Zhang, et al. No fear of heterogeneity: Classifier calibration for federated learning with non-iid data. In *NeurIPS*, pages 5972–5984, 2021. 1
- [34] Caron Mathilde, Hugo Touvron, Ishan Misra, Hervé Jégou, et al. Emerging properties in self-supervised vision transformers. In *ICCV*, pages 9650–9660, 2021. 8
- [35] Brendan McMahan, Eider Moore, Daniel Ramage, Seth Hampson, et al. Communication-efficient learning of deep networks from decentralized data. In *AISTATS*, pages 1273–1282, 2017. 1, 2, 7, 9
- [36] Matias Mendieta, Taojiannan Yang, Pu Wang, Minwoo Lee, et al. Local learning matters: Rethinking data heterogeneity in federated learning. In *CVPR*, pages 8397–8406, 2022. 1, 3
- [37] John Nguyen, Kshitiz Malik, Hongyuan Zhan, Ashkan Yousefpour, et al. Federated learning with buffered asynchronous aggregation. In *AISTATS*, pages 3581–3607, 2022. 2
- [38] Alexander Quinn Nichol and Prafulla Dhariwal. Improved denoising diffusion probabilistic models. In *ICML*, pages 8162–8171, 2021. 2, 3
- [39] Aaron van den Oord, Yazhe Li, and Oriol Vinyals. Representation learning with contrastive predictive coding. In *NeurIPS*, 2019. 3
- [40] Reese Pathak and Martin J Wainwright. Fedsplit: An algorithmic framework for fast federated optimization. In *NeurIPS*, pages 7057–7066, 2020. 2
- [41] Helber Patrick, Benjamin Bischke, Andreas Dengel, and Damian Borth. Eurosat: A novel dataset and deep learning

- benchmark for land use and land cover classification. *IEEE J-STARS*, 12(7):2217–2226, 2019. 8, 9
- [42] Xingchao Peng, Qinxun Bai, Xide Xia, Zijun Huang, et al. Moment matching for multi-source domain adaptation. In *ICCV*, pages 1406–1415, 2019. 7, 13, 14
- [43] Athanasios Psaltis, Anestis Kastellos, Charalampos Z Patrikakis, and Petros Daras. Fedlid: Self-supervised federated learning for leveraging limited image data. In *ICCV*, pages 1039–1048, 2023. 7, 13
- [44] Pian Qi, Diletta Chiaro, Antonella Guzzo, Michele Ianni, et al. Model aggregation techniques in federated learning: A comprehensive survey. *Future Generation Computer Systems*, 150:272–293, 2024. 3
- [45] Liangqiong Qu, Yuyin Zhou, Paul Pu Liang, Yingda Xia, et al. Rethinking architecture design for tackling data heterogeneity in federated learning. In *CVPR*, pages 10061–10071, 2022. 1
- [46] Alec Radford, Jong Wook Kim, Chris Hallacy, Aditya Ramesh, et al. Learning transferable visual models from natural language supervision. In *ICML*, pages 8748–8763, 2021. 8
- [47] Robin Rombach, Andreas Blattmann, Dominik Lorenz, Patrick Esser, et al. High-resolution image synthesis with latent diffusion models. In *CVPR*, pages 10684–10695, 2022. 2, 3, 5, 16
- [48] Olaf Ronneberger, Philipp Fischer, and Thomas Brox. U-net: Convolutional networks for biomedical image segmentation. In *MICCAI*, pages 234–241, 2015. 2, 3, 4
- [49] Mark Sandler, Andrew Howard, Menglong Zhu, Andrey Zhmoginov, et al. Mobilenetv2: Inverted residuals and linear bottlenecks. In *CVPR*, pages 4510–4520, 2018. 7, 13
- [50] Christoph Schuhmann, Romain Beaumont, Richard Vencu, Cade Gordon, et al. Laion-5b: An open large-scale dataset for training next generation image-text models. In *NeurIPS*, pages 25278–25294, 2022. 9
- [51] Seonguk Seo, Jinkyu Kim, Geeho Kim, and Bohyung Han. Relaxed contrastive learning for federated learning. In *CVPR*, pages 12279–12288, 2024. 7, 13
- [52] Fiona Victoria Stanley Jothiraj and Afra Mashhadi. Phoenix: A federated generative diffusion model. In *ACM WWW*, pages 1568–1577, 2024. 3
- [53] Yue Tan, Guodong Long, Lu Liu, Tianyi Zhou, et al. Fed-proto: Federated prototype learning across heterogeneous clients. In *AAAI*, pages 8432–8440, 2022. 3, 7, 13
- [54] Yue Tan, Guodong Long, Jie Ma, Lu Liu, et al. Federated learning from pre-trained models: A contrastive learning approach. In *NeurIPS*, pages 19332–19344, 2022. 3
- [55] Luming Tang, Menglin Jia, Qianqian Wang, Cheng Perng Phoo, et al. Emergent correspondence from image diffusion. In *NeurIPS*, pages 1363–1389, 2023. 3
- [56] Yonglong Tian, Chen Sun, Ben Poole, Dilip Krishnan, et al. What makes for good views for contrastive learning? In *NeurIPS*, pages 6827–6839, 2020. 3
- [57] Philipp Tschandl, Cliff Rosendahl, and Harald Kittler. The ham10000 dataset, a large collection of multi-source dermatoscopic images of common pigmented skin lesions. *Nature Scientific Data*, 5(1):1–9, 2018. 8, 9
- [58] Laurens van der Maaten and Geoffrey Hinton. Visualizing data using t-sne. *Journal of Machine Learning Research*, 9(86):2579–2605, 2008. 16
- [59] Laurens Van der Maaten and Geoffrey Hinton. Visualizing data using t-sne. *Journal of Machine Learning Research*, 9(11):2579–2605, 2008. 4
- [60] Feng Wang and Huaping Liu. Understanding the behaviour of contrastive loss. In *CVPR*, pages 2495–2504, 2021. 2
- [61] Hongyi Wang, Mikhail Yurochkin, Yuekai Sun, Dimitris Papailiopoulos, et al. Federated learning with matched averaging. In *ICLR*, 2020. 7
- [62] Haozhao Wang, Haoran Xu, Yichen Li, Yuan Xu, et al. Fed-cda: Federated learning with cross-rounds divergence-aware aggregation. In *ICLR*, 2024. 3, 7
- [63] Yingheng Wang, Yair Schiff, Aaron Gokaslan, Weishen Pan, et al. Infodiffusion: Representation learning using information maximizing diffusion models. In *ICML*, pages 36336–36354, 2023. 4
- [64] Yuan Wang, Huazhu Fu, Renuga Kanagavelu, Qingsong Wei, et al. An aggregation-free federated learning for tackling data heterogeneity. In *CVPR*, pages 26233–26242, 2024. 3
- [65] Chen Wei, Kartikeya Mangalam, Po-Yao Huang, Yanghao Li, et al. Diffusion models as masked autoencoders. In *ICCV*, pages 16284–16294, 2023. 3
- [66] Weilai Xiang, Hongyu Yang, Di Huang, and Yunhong Wang. Denoising diffusion autoencoders are unified self-supervised learners. In *ICCV*, pages 15802–15812, 2023. 3
- [67] Yikai Yan, Chaoyue Niu, Yucheng Ding, Zhenzhe Zheng, et al. Federated optimization under intermittent client availability. *INFORMS Journal on Computing*, 36(1):185–202, 2024. 2
- [68] Ling Yang, Zhilong Zhang, Yang Song, Shenda Hong, et al. Diffusion models: A comprehensive survey of methods and applications. *ACM Computing Surveys*, 56(4):1–39, 2023. 3
- [69] Mingzhao Yang, Shangchao Su, Bin Li, and Xiangyang Xue. Exploring one-shot semi-supervised federated learning with pre-trained diffusion models. In *AAAI*, pages 16325–16333, 2024. 3, 9
- [70] Xingyi Yang and Xinchao Wang. Diffusion model as representation learner. In *ICCV*, pages 18938–18949, 2023. 4
- [71] Rui Ye, Mingkai Xu, Jianyu Wang, Chenxin Xu, et al. Fed-disco: Federated learning with discrepancy-aware collaboration. In *ICML*, pages 39879–39902, 2023. 2, 3, 6, 7, 9
- [72] Dai Yutong, Zeyuan Chen, Junnan Li, Shelby Heinecke, et al. Tackling data heterogeneity in federated learning with class prototypes. In *AAAI*, pages 7314–7322, 2023. 7, 13
- [73] Daokun Zhang, Jie Yin, Xingquan Zhu, and Chengqi Zhang. Network representation learning: A survey. *IEEE Transactions on Big Data*, 6:3–28, 2018. 4
- [74] Junyi Zhang, Charles Herrmann, Junhwa Hur, Luisa Polania Cabrera, et al. A tale of two features: Stable diffusion complements dino for zero-shot semantic correspondence. In *NeurIPS*, 2023. 3
- [75] Jianqing Zhang, Yang Hua, Hao Wang, Tao Song, et al. Fedala: Adaptive local aggregation for personalized federated learning. In *AAAI*, pages 11237–11244, 2023. 2, 3

- [76] Zhuang Zhao, Feng Yang, and Guirong Liang. Federated learning based on diffusion model to cope with non-iid data. In *PRCV*, pages 220–231, 2023. [3](#), [9](#)
- [77] Hangyu Zhu, Jinjin Xu, Shiqing Liu, and Yaochu Jin. Federated learning on non-iid data: A survey. *Elsevier Neurocomputing*, 465:371–390, 2021. [1](#)
- [78] Fuzhen Zhuang, Xiaohu Cheng, Ping Luo, Sinno Jialin Pan, et al. Supervised representation learning: Transfer learning with deep autoencoders. In *IJCAI*, 2015. [4](#)
- [79] Weiming Zhuang, Yonggang Wen, and Shuai Zhang. Divergence-aware federated self-supervised learning. In *ICLR*, 2022. [7](#)